Front. Optoelectron. 2020, 13(3): 196–224
https://doi.org/10.1007/s12200-020-1039-6

REVIEW ARTICLE

Dimensionality engineering of metal halide perovskites

Rashad F. KAHWAGI, Sean T. THORNTON, Ben SMITH, Ghada I. KOLEILAT (✉)

Department of Chemical Engineering, Dalhousie University, Halifax, Nova Scotia, B3J 1Z1, Canada

Abstract Metal halide perovskites are a class of materials that are ideal for photodetectors and solar cells due to their excellent optoelectronic properties. Their low-cost and low temperature synthesis have made them attractive for extensive research aimed at revolutionizing the semiconductor industry. The rich chemistry of metal halide perovskites allows compositional engineering resulting in facile tuning of the desired optoelectronic properties. Moreover, using different experimental synthesis and deposition techniques such as solution processing, chemical vapor deposition and hot-injection methods, the dimensionality of the perovskites can be altered from 3D to 0D, each structure opening a new realm of applications due to their unique properties. Dimensionality engineering includes both morphological engineering–reducing the thickness of 3D perovskite into atomically thin films–and molecular engineering–incorporating long-chain organic cations into the perovskite mixture and changing the composition at the molecular level. The optoelectronic properties of the perovskite structure including its band gap, binding energy and carrier mobility depend on both its composition and dimensionality. The plethora of different photodetectors and solar cells that have been made with different compositions and dimensions of perovskite will be reviewed here. We will conclude our review by discussing the kinetics and dynamics of different dimensionalities, their inherent stability and toxicity issues, and how reaching similar performance to 3D in lower dimensionalities and their large-scale deployment can be achieved.

Keywords optoelectronics, solar cells, perovskite, photodetectors, metal halides, dimensionality

1 Introduction

Perovskites–named after Russian mineralogist L.A. Perovski–originate from the discovery of calcium titanate ($CaTiO_3$) in the 1830s by Gustav Rose [1,2]. The definition of perovskites has since been extended to include all compounds with a similar crystal structure to $CaTiO_3$ [2,3]. Recently, metal halide perovskites have emerged as a promising class of materials for many applications such as solar cells, photodetectors, and LEDs due to their low-cost, low temperature synthesis and solution processability [2,4]. Metal halide perovskites exhibit excellent optoelectronic properties including small exciton binding energy, bandgap tunability, high charge carrier mobility [5], long charge carrier diffusion length [6], high absorption coefficients and broad spectral absorption [7]. Ever since Miyasaka et al. first made sensitized photovoltaic cells (PVs) in 2009 from metal halide perovskites, progress in power conversion efficiencies (PCEs) of perovskite-based PVs has jumped from around 4%, to over 22% [1,2,6,7] and now currently over 25% [8]. Additionally, there has been vast progress in utilizing perovskites in photodetector and other optoelectronic applications making them a promising candidate to bring about a new paradigm in the semiconductor industry [1–6].

Metal halide perovskites have the chemical formula ABX_3, where A and B are cations of different size and X is a halide anion [2,3,6,7,9]. The composition of the perovskite structure can be readily changed to manipulate the photophysical properties of the material [1–5]. For example, the halide composition can be tuned to achieve the desired spectral response ranging from the UV all the way to the near infrared [9,10]. Apart from compositional engineering, dimensional engineering of the perovskite can also be achieved [1–6]. For example, by including different compositions of organic acids and amines as the cations, the shape and dimensionality of the perovskite can be altered to form 3D nanocubes, 2D nanoplatelets, 1D nanorods, and 0D quantum dots [2,3,9]. In addition to morphological control of the perovskites, their dimensionality can be tuned at the molecular level: quasi-2D perovskites with enhanced stability can be created by incorporating bulky organic cations into the conventional 3D perovskite mixture [1–7]. Further lowering of the

Received April 14, 2020; accepted June 22, 2020

E-mail: ghada.koleilat@dal.ca

dimensionality at the molecular level leads to further exciton self-trapping and structural distortion [1–3]. In the most extreme cases, true 0D hybrid structures can be formed where the metal halide clusters are completely separated by organic moieties [1–3,6]. In this review, the different morphological and molecular engineering techniques used to manipulate the structural characteristics of perovskites and the corresponding changes to the optoelectronic characteristics will be explored. We will also detail the recent progress of photodetectors and solar cells employing the different perovskite structures. Finally, we will discuss the next steps forward that need to be investigated for this class of material.

2 Properties and characteristics

2.1 Structure and dimensionality

Metal halide perovskites are typically processed using simple wet-chemistry methods to allow homogeneous mixing at the molecular level and the production of a pure phase solution [10–13]. The extensive library of chemicals that can be used in the perovskite solution enables intricate compositional engineering and tuning of the desired optoelectronic properties [14–24]. Typically, the precursors are mixed in a polar aprotic solvent (e.g., DMSO, DMF) and deposited onto a substrate [25,26]. Deposition of the mixture is performed using methods including spin-coating, dip-coating, inkjet printing and blade coating [27–29]. There is an exceptionally low energy barrier for the formation of halide perovskites, which means they can crystallize at relatively low temperatures [10]. The quality and age of the chemicals, the concentration and stoichiometry of the precursors [10], the atmospheric conditions of the reaction [9,10], the substrate of the perovskite is grown onto and other factors will have an effect on the thin-film morphology, which is in turn directly linked to the optoelectronic properties of the fabricated films [10,25,27].

Moreover, reducing the dimensionality at both the morphological and molecular levels can lead to further tuning of the optoelectronic properties [2,3,9,30]. Morphological low-dimensional perovskites include 2D nanoplatelets, 1D nanorods and nanowires, and 0D quantum dots [2,3,9]. These perovskites are formed by reducing the thickness of 3D perovskite into atomically thin films [2,3,9,31]. These structures, while identical in crystal structure to 3D perovskites, are on the nanoscale and exhibit quantum confinement in at least one dimension [2,3,5,6,12]. On the other hand, lowering the dimensionality at the molecular level leads to hybrid structures composed of metal halide layers separated by long-chain hydrophobic organic cations [3,5,7,8,12]. These structures display quantum confinement effects without small atomic thicknesses and can be described as a series of naturally integrated quantum wells [31,32]. The bulky organic cations provide inherent hydrophobicity, making molecular low-dimensional perovskites promising candidates for stable optoelectronic devices [3,5,7,8,12]. The difference between molecular and morphological low-dimensional perovskite structures is displayed in Fig. 1 [2,3].

The crystal structure of each dimensionality of perovskite will be discussed first to illustrate how it contributes to the plethora of remarkable optoelectronic properties for the different forms of the material [2–4,10].

2.1.1 3D Perovskites

The ionic structure of 3D perovskites can be described by the general formula ABX_3 [6,12,21,25,33], where each element is distributed spatially as depicted in Fig. 2 [33].

A is typically a monovalent cation (e.g., $CH_3NH_3^+$ or MA^+, FA^+ or Cs^+); B is a divalent cation (e.g., Pb^{2+}, Sn^{2+}, Cu^{2+}) and X is a halide anion (e.g., Cl^-, Br^-, I^-) that binds to the A and B sites [13,34,35]. In a 3D perovskite system, the A-site cations occupy the space in between four adjacent corner-sharing BX_6 octahedra [6,9]. To be classified as a perovskite, the ions constituting the crystal must meet requirements regarding their size and charge, best described by the Goldschmidt tolerance factor (t):

$$t = (r_A + r_X)/\left(\sqrt{2}(r_B + r_X)\right), \quad (1)$$

where r is the atomic radii of the A, B and X ions [3,9].

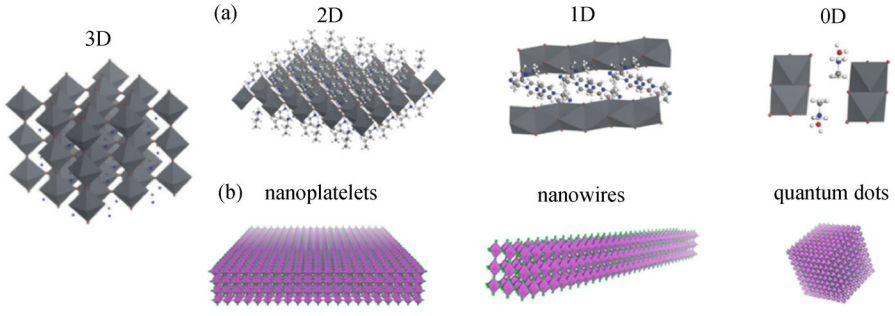

Fig. 1 3D perovskite. (a) Low-dimensional perovskite hybrids. Reprinted with permission from Ref. [3], Copyright 2018, Royal Society of Chemistry. (b) Morphological low-dimensional perovskites. Reprinted with permission from Ref. [2], Copyright 2019, Elsevier

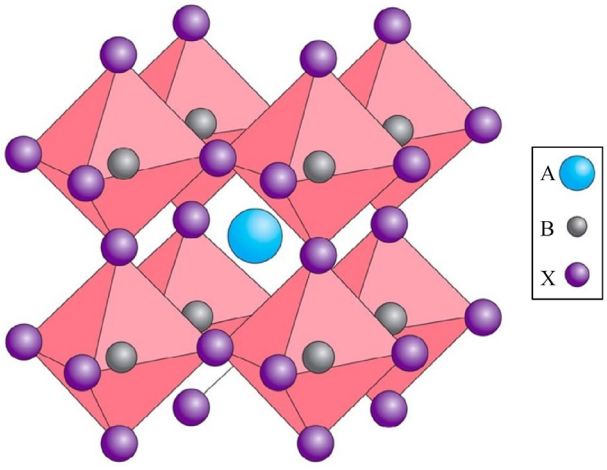

Fig. 2 Perovskite crystal structure, showing the position of the A, B and X ion sites. Reprinted with permission from Ref. [33], Copyright 2014, Springer Nature

The tolerance factor should be close to 1 for a stable 3D perovskites structure [31]. Perovskites can adopt a multitude of crystal structures including cubic (for a tolerance factor between 0.8 and 0.9), orthorhombic, rhombohedral, and tetragonal based on the size of the constituting ions [10] as well as the ambient thermal conditions [10,36].

The most heavily researched 3D perovskite structure is methylammonium lead iodide ($MAPbI_3$), which consists of a monovalent cation (MA^+), a divalent metallic cation (Pb^{2+}) and halogenic anions (I^-) [10]. Unfortunately, organic-inorganic perovskites such as $MAPbI_3$ mainly suffer from poor long-term stability when exposed to light, moisture, and heat as a result of weak chemical bonding between the structural components, resulting in degradation to PbX_2 [18,37]. To avoid this, completely inorganic perovskites are being investigated that do not degrade as readily [18]. $CsPbX_3$ is an example of a completely inorganic 3D perovskite being investigated extensively as a result of its promising applications in solar cells and inherent stability [21,26,38].

2.1.2 2D perovskites

Low-dimensional perovskites such as 2D perovskite are garnering interest because of their unique optical and charge transport properties and improved stability [39]. 2D perovskites are formed by reducing the thickness of 3D perovskite (morphological engineering) or adding bulky organic cations to the mixture (molecular engineering) [2,5,31]. Inherently, molecular 2D perovskites are more resistant to moisture because of the hydrophobic organic components and their highly oriented, densely packed nature, which prevents the formation of hydrates [2,12,31,40,41]. Furthermore, the organic components can be engineered to be flexible [5,20]. As such, 2D perovskites are expected to produce large-scale, stable, and flexible optoelectronics in the future [5]. However, performance, particularly efficiency, remains lower than their 3D counterparts [2,7,42] due to their wider band gap and intrinsic anisotropic charge transport along the conductive layers [5,40].

Morphological 2D metal halide perovskites are formed by reducing the thickness of 3D perovskite to form nanosheets, nanoplatelets and nanodisks [43–46]. Examples of morphological 2D perovskites are shown in Fig. 3 [13,44,45].

2D perovskite nanoplatelets have been garnering attention as a result of their interesting optical and electronic properties. The excitons are bound more strongly together in this type of structure because they are confined to a 2D plane [46]. These types of perovskites have been formed using chemical vapor deposition (CVD) and solution processing methods including the solid state crystallization method [47], exfoliation method [48], hot-injection crystallization method [13], and non-solvent crystallization method [46,48]. Ha et al. grew 2D perovskite nanoplatelets

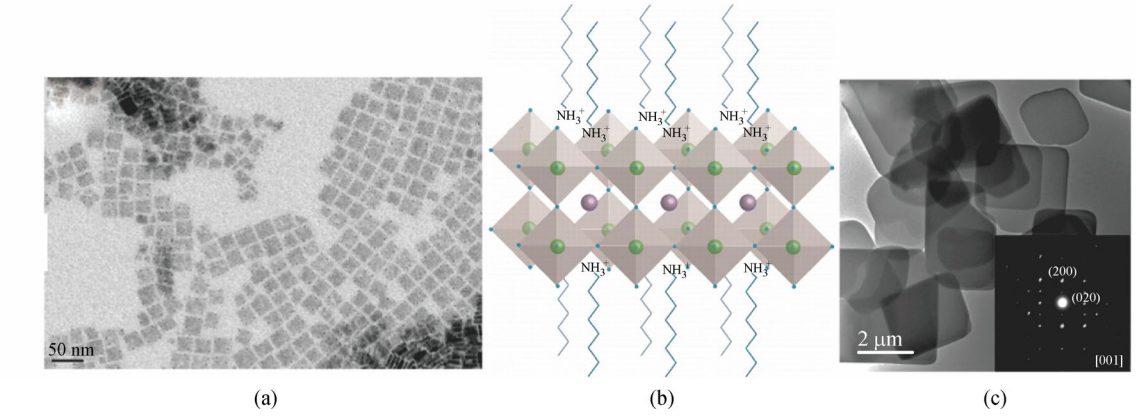

Fig. 3 (a) TEM image of 2D perovskite nanosheet. Reprinted with permission from Ref. [44], Copyright 2016, American Chemical Society. (b) Schematic showing the structure of 2D perovskite nanoplatelet. Reprinted with permission from Ref. [13], Copyright 2015, American Chemical Society. (c) TEM image of 2D perovskite nanodisk. Reprinted with permission from Ref. [45], Copyright 2015, Royal Society of Chemistry

($MAPbI_3$) using CVD and the novel structures showed higher electron diffusion lengths (200 nm) than their solution-processed counterparts [49]. Furthermore, solution-processable 2D perovskite ($MAPbBr_3$) nanoplatelets resulting in bright LEDs were developed by Ling and coworkers [39]. The nanoplatelets in this later report were synthesized using a facile one-pot synthesis method and resulted in LEDs with quantum yields over 85% [39]. Furthermore, 2D $MAPbBr_3$ nanoplatelets with almost single unit cell thickness, submicron lateral dimensions and a blue-shifted sharp excitonic absorption feature were recently created by Tyagi and coworkers [13] using a simple colloidal synthesis method developed by Schmidt et al. [50]. This work demonstrated that excitonic features previously attributed to quantum confinement in $MAPbBr_3$ nanoplatelets are in fact a property of the bulk perovskite phase [13].

Molecular 2D perovskites on the other hand are formed by isolating the lead halide octahedral sheets with long-chain organic cations [21,35]. As a result, molecular 2D perovskites exhibit higher stability and higher band gaps and exciton binding energies as a result of the quantum and dielectric confinement effects that arise from the bulky organic cations [9,17]. Furthermore, the bulky organic cations greatly decrease the conductivity in the plane perpendicular to the inorganic perovskite lattice [5,40]. Molecular level 2D perovskites are separated into two categories: pure and quasi-2D where the distinction arises from the number of octahedra sheets sandwiched between two organic interlayers (n) [2,6]. Pure 2D structures possess a single layer (with $n = 1$) while quasi-2D structures have more layers (where $1 < n < \infty$) [2,5,6], as shown in Fig. 4 [21].

Research into molecular 2D perovskite has significantly increased in recent years due to their inherent stability and unique optoelectronic properties [2,42]. Solution-processing methods (e.g., spin-coating) are the most popular methods to fabricate 2D perovskites because of their simplicity and effectiveness in growing relatively large crystals [2,9,51]. Pure 2D perovskites possess the formula of A'_2BX_4, where A′ is the long hydrophobic alkyl chain, B is the divalent metal and X is the halide [21,23]. Many bulky organic cations have been incorporated into pure 2D perovskite including butyl-ammonium (BA) [21], pentylammonium (PentA) [6], and 2-phenylethylammonium (PEA) [52,53]. $(PEA)_2SnI_4$ is an example of a pure-2D perovskite that has been created and has been tested in devices such as solar cells and photodetectors [20,34].

Quasi-2D perovskite is formed by incorporating another long organic molecule into a 3D perovskite mixture [5,21,54]. It has a general formula of $A_{n-1}A'_2B_nX_{3n+1}$, where A′ is a large monovalent organic cation, A is a small cation present in the inorganic framework, B is a divalent metal cation and X is a halide [2,20,55,56]. The long organic cation A'^{+} must contain a functional group that can react ionically with the inorganic and anionic perovskite lattice but not with the A organic cation [31]. In quasi-2D perovskite, the layers of BX_6 octahedra are found sandwiched between the long organic cation chains [31,41,55–61], as depicted in Fig. 4 [5]. The long organic cations serve as a natural encapsulation layer that blocks the infiltration of water and oxygen into the grain boundaries thereby increasing the stability of the structure [7,56]. The Coulombic and hydrophobic forces between the organic and inorganic layers maintains the integrity of the structure [62,63]. The alternating inorganic and organic layers present form a large assembly of quantum wells, leading to improved overall insulation and long-term stability [4,31].

The long cations that are used in this type of perovskite are typically n-butyl-ammonium (n-BA^+) and 2-phenylethylammonium (PEA^+) [20,21,31,34]. In quasi-2D perovskite, the interlayer interaction between adjacent perovskite sheets is mediated by weak van der Waals and hydrogen bonding between the bulky organic cations [62]. Recently, Ren et al. used $MTEA^+$ (2-(methylthio)ethylammonium) as the bulky A′ cation in a certified 17.8% PCE quasi-2D perovskite solar cell. As shown in Fig. 5, the additional sulfur-sulfur interaction between the MTEA molecules strengthened the stability of the device immensely when compared to a BA^+ based quasi-2D perovskite [62]. The solar cell showed incredible moisture tolerance

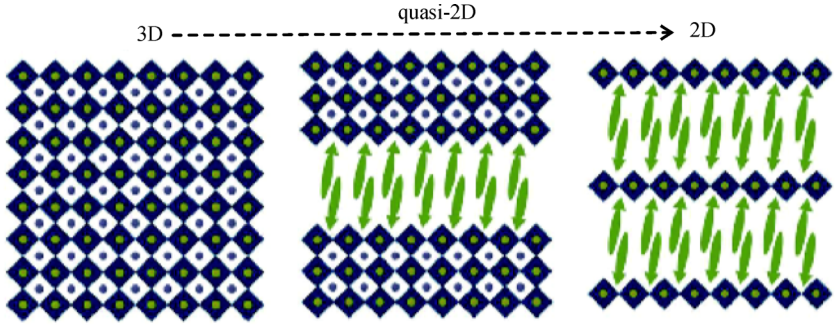

Fig. 4 Perovskite lattices with different dimensions, on the left: 3D perovskite ($n = \infty$), in the middle: quasi-2D perovskite ($1 < n < \infty$) and on the right: pure 2D perovskite ($n = 1$). Reprinted with permission from Ref. [5], Copyright 2018, Springer Nature

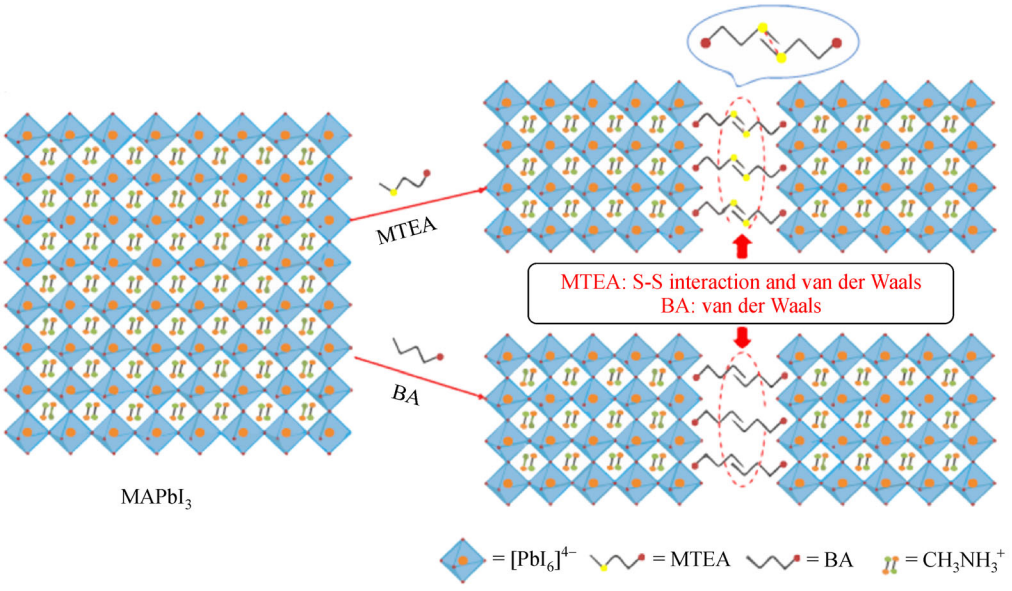

Fig. 5 Schematic crystal structures of the quasi-2D perovskites $(MTEA)_2(MA)_{n-1}Pb_nI_{3n+1}$ and $(BA)_2(MA)_{n-1}Pb_nI_{3n+1}$. Reprinted with permission from Ref. [62], Copyright 2020, Springer Nature

(no change in XRD trace after 1512 h under 70% humidity conditions) [62].

Various examples of organic cations used in quasi-2D perovskite along with their potential applications and performance are shown in Table 1. It is important to note that while 2D are promising in their versatility and various utility, they have not yet reached over 20% efficiency like their 3D counterparts [8].

Quasi-2D perovskites have inherently larger inorganic layer thickness than pure-2D perovskites. The number of octahedra sheets in between organic layers (n) controls the bandgap of the material [37,74–76]. As such, many approaches have been used in an attempt to control the number of inorganic layers (n) from adjusting the ratio of the A′ to A organic molecules [5] to carefully controlling the reaction/crystallization conditions (e.g., hot-casting) [20,41,42,74].

In addition to pure quasi-2D perovskite crystals with fixed n numbers, there has been investigations into perovskites with multiple phases and varied n numbers [77,78]. Recently, using a liquid phase crystallization method, Liu et al. created a film of $(BA)_2(MA)_{n-1}Pb_nI_{3n+1}$ with $n = 2$ to approximately $n = \infty$, which naturally aligns in order of n in the direction perpendicular to the substrate, as seen in Fig. 6 [77]. As shown in Fig. 6, n increases from 2 to ∞ as the perovskite film progresses away from the substrate [77]. This band alignment of the perovskite phases can potentially lead to improved charge extraction efficiency, because the electrons and holes are driven to opposite ends of the films [77].

To summarize, 2D perovskite can be obtained by morphological or molecular engineering [2,5,31]. 2D perovskites show enhanced stability and flexibility, leading to the idea that they will be readily produced on a large-scale soon [5]. Furthermore, the enhanced excitonic binding energy shown in morphological 2D perovskite leads to unique properties useful in specific applications, such as LEDs with high quantum yields [39]. Molecular 2D perovskites, on the other hand, can be pure ($n = 1$) or quasi-2D ($n = 2$ to $n = \infty$), depending on depending on the number of octahedra sheets sandwiched in between the organic layers [31,41,54–61,69]. Many organic molecules have been used in quasi-2D perovskite, leading to increased stability and performance that is quickly approaching that of 3D perovskites [70]. Finally, engineering the number of octahedra sheets (n) in between the organic interlayers may lead to better charge transport that can translate directly to enhanced device efficiency [77].

2.1.3 1D perovskites and hybrids

Lowering the dimensionality further to 1D can lead to even more exciton self-trapping and structural distortion [1,2,9].

1D nanostructures such as nanowires and nanorods have demonstrated remarkable optical properties because of their higher crystallinity, lower recombination rate, and longer carrier diffusion lengths and lifetimes [6,79–81]. Many experimental methods have been developed to synthesize 1D perovskite nanowires including vapor phase methods and solution phase methods [82–84]. For example, Xing et al. created free-standing, single crystalline $MAPbI_3$, $MAPbBr_3$ and $MAPbI_xCl_{3-x}$ nanowires using a two-step vapor phase synthesis method [85]. In

Table 1 A list of organic cations used in quasi-2D perovskites with their potential optoelectronic applications

organic cation	example perovskite	device	PCE	Ref.
n-BA^+/*n*-butyl-ammonium	$(BA)_2(MA)_3Pb_4I_{13}$	solar cell	12.52	[57]
	$(BA)_n(MA)_{n-1}Pb_nI_{3n+1}$	solar cell	17.26	[64]
	$BA_2MA_{n-1}Sn_nI_{3n+1}$	photodetector	–	[58]
		solar cell		[65]
PEA^+/2-phenylethylammonium	$(PEA)_2(MA)_{n-1}Pb_nI_{3n+1}$	solar cell	15.3	[59]
	$(PEA)_2Ge_{1-n}Sn_nI_4$	solar cell	–	[66]
	$(PEA)_2(MA)_{n-1}Pb_nBr_{3n+1}$	LED	–	[67]
PDA^+/propane–1,3-diammonium	$PDAMA_{n-1}Pb_nI_{3n+1}$	solar cell	13.0	[51]
$C(NH_2)_3^+$/guanidinium	$(C(NH_2)_3)(CH_3NH_3)_nPb_nI_{3n+1}$ (n = 1, 2, 3)	solar cell	7.26	[68]
BDA^+/1,4–butanediammonium	$BDAMA_{n-1}Pb_nX_{3n+1}$	solar cell	17.91	[54]
NMA^+/naphthylmethylammonium	$(NMA)_2(FA)Pb_2I_6Br$	LED	–	[69]
$3AMP^+$/3-(aminomethyl)piperidinium	$(3AMP)(MA)_3Pb_4I_{13}$	solar cell	12.04	[56]
$C_6H_5CH_2NH_3^+$	$(C_6H_5CH_2NH_3)_2(FA)_8Pb_9I_{28}$	solar cell	17.40	[70]
PEI^+/polyethyleneimine	$(PEI)_2(MA)_{n-1}Pb_nI_{3n+1}$	solar cell	8.77	[71]
$ThMA^+$/2-thiophenemethylammonium	$(ThMA)_2(MA)_{n-1}Pb_nI_{3n+1}$	solar cell	15.42	[72]
ALA^+/allylammonium	$(ALA)_2(MA)_{n-1}Pb_nI_{3n-1}$	solar cell	16.5	[73]
$MTEA^+$/2-(methylthio)ethylammonium	$(MTEA)_2(MA)_4Pb_5I_{16}$	solar cell	17.8	[62]

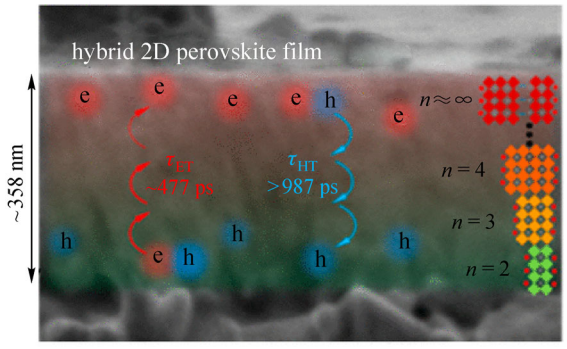

Fig. 6 Multilayered 2D hybrid perovskite ($(BA)_2(MA)_{n-1}Pb_nI_{3n+1}$) film showing the enhanced charge transport because of the $n = 2$ to $n = \infty$ layering. The film is approximately 358 nm thick. The electron transport time is approximately 477 ps and the hole transfer time is approximately 987 ps. Reprinted with permission from Ref. [77], Copyright 2017, American Chemical Society

comparison, perovskite nanorods are rarely created using the vapor phase method and are typically created using other techniques such as solution phase and hot-injection methods [50,86]. Using a solution phase method, Yang and coworkers were able to create stable $MAPbBr_3$ nanorod arrays in ambient conditions [87].

In molecular 1D perovskite hybrids, the metal halide octahedra BX_6 form chains by sharing corners, edges or faces with each other. The metal halide chains are then united with the surrounding organic cations to form the single crystal bulk structures. In contrast to morphological 1D perovskites, molecular level 1D perovskite hybrids are not nanomaterials [88], but large crystals with 1D structure that are effectively bulk assemblies of metal halide quantum wires [2]. For instance, a 1D lead halide hybrid $C_4N_2H_{14}PbBr_4$ that emits efficient bluish white-light has been created where edge-sharing octahedral chains [$PbBr_4^{2-}$] are surrounded by $C_4N_2H_{14}^{2+}$ organic cations, as shown in Fig. 7 [89].

Moreover, recently, Jung created zigzag edge-sharing molecular 1D perovskites ($(AMP)PbCl_4$, AMP = $C_6H_{10}N_2$) that exhibited efficient white-light emission with a high color rendering index of 90.21 [90]. Interestingly, these 1D crystals can also be formed of multiple different metal halide chains [2].

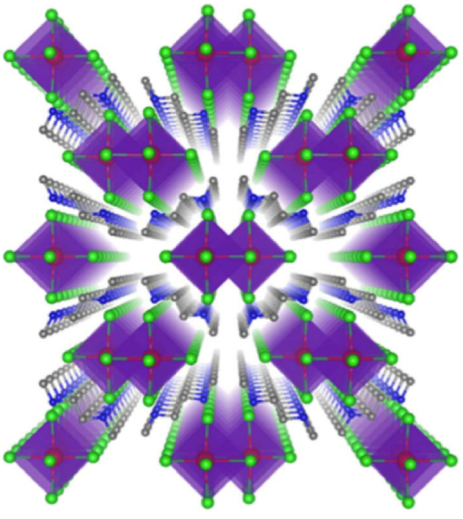

Fig. 7 Structure of 1D perovskite ($C_4N_2H_{14}PbBr_4$) showing [$PbBr_4^{2-}$] octahedra surrounded by $C_4N_2H_{14}^{2+}$ organic cations [89]

2.1.4 0D perovskites and hybrids

Morphological 0D perovskites–0D nanocrystals–often exhibit enhanced optoelectronic properties in comparison to their bulk counterparts because of their large surface to volume ratio, strong quantum confinement, and anisotropic geometry. They have attracted lots of research attention largely because of their simple synthesis and enhanced stability [2]. Numerous methods have been used to create 0D nanocrystals including ligand-assisted reprecipitation (LARP) [50,91], *in situ* preparation [92,93] and hot-injection techniques [24]. Furthermore, recently Liu et al. used a solution processing method to create $FAPbBr_3$ nanocrystals with linearly polarized photoluminescence, which could lead to applications in photodetectors, LEDs, and lasers [94].

Molecular level 0D perovskite hybrids feature isolated metal halide polyhedrons encased with organic or inorganic cations. In this case, the bulk crystals demonstrate the inherent properties of the individual metal halide polyhedra [2]. The first report of this type of perovskite hybrid was Cs_4PbBr_6, which features $PbBr_6$ octahedrons separated by inorganic Cs^+ cations [95]. Since then, other types of molecular 0D perovskite hybrids have been investigated featuring large-sized organic cations between neighboring octahedra, thereby enhancing electronic confinement [96,97]. Taking advantage of their high photoluminescence quantum efficiency (PLQE) and emission color tunability [98], these materials have great potential as phosphors in down-conversion white LEDs [2]. They have also been investigated for use in solar cells [99,100], however the efficiencies were low in comparison to 3D perovskite because of strong confinement of charge in the metal halide clusters. These 0D structures also have potential as efficient capacitors because of the large empty surface area present inside the crystals. For instance, a capacitor has been demonstrated with 0D $(CH_3NH_3)_3Bi_2I_9$ that has three orders of magnitude higher capacitance than the standard $MAPbI_3$ perovskite [101].

2.2 Optoelectronic properties

Implementing technology is at the heart of all materials research, and perovskite's inherent promising optoelectronic properties put it in a great position to be a potential game changer in the development of next generation of devices. The following section will discuss the unique optoelectronic properties of halide perovskite materials, from their tunable bandgaps, impressive carrier mobilities and high absorption coefficients, to long diffusion lengths and low exciton binding energies [102–104].

2.2.1 Bandgap engineering

The optical bandgap of a material provides a window into its electrical potential by shedding some light on certain properties such as the absorption range and the upper theoretical limit of the open-circuit voltage [104]. Two types of bandgaps can be found in semiconductors: direct and indirect. The distinction is made by plotting the material's light absorption energy values against the crystal momentum and observing the minimum conduction and maximum valence band values [105]. Ideally, the majority of incident photons are harvested with minimal loss, and an equal momentum value is obtained for both maximum and minimum band values, indicating that the material possesses a direct bandgap. On the other hand, light may need to interact with phonons first before absorption, which is the case with indirect bandgap materials. This will decrease the chance of harvesting light energy. As a result, indirect bandgap materials must be thicker (100 μm) than direct bandgap materials (< 1 μm) [10,105,106].

There has been much debate regarding the nature of bandgaps in lead halide perovskites [39,42,106–112]. A study conducted by Kandada et al. showed that perovskite materials possess an indirect bandgap by highlighting the need for a momentum higher than a photon to trigger a recombination [39,112]. On the other hand, Sarritzu's team tested the bandgaps in hybrid lead halide perovskites [107]. The results showed an increase in radiative recombination rates with decreasing temperature. This is a feature of direct bandgap materials [107,109,110]. Researchers also demonstrated that metal halide perovskites such as $MAPbI_3$ may in fact possess direct-indirect bandgap characteristics in their tetragonal phase as depicted in Figs. 8(a) and 8(b) [108,111]. A clear comparison between different perovskite compositions and their respective bandgaps can be seen in Fig. 9.

3D perovskite bandgaps can be tuned by modifying their

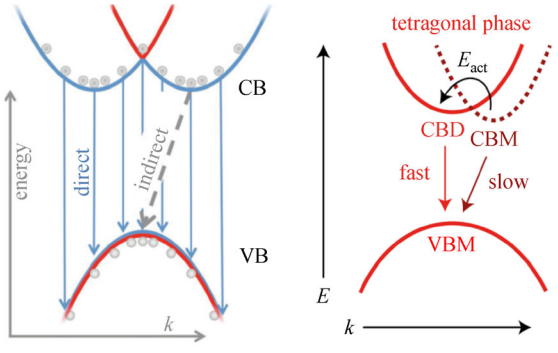

Fig. 8 Highlighting the direct-indirect nature of the perovskite bandgap with (a) Rashba spin-orbit coupling effect on optical transition. Reprinted with permission from Ref. [107], Copyright 2018, Wiley. (b) Proposed band diagram for the perovskite's tetragonal phase with a slightly shifted conduction band minimum (CBM) compared to the valence band maximum (VBM), highlighting the indirect bandgap, while the minimum in conduction band showing the direct bandgap (CBD). Reprinted with permission from Ref. [108], Copyright 2017, Springer Nature

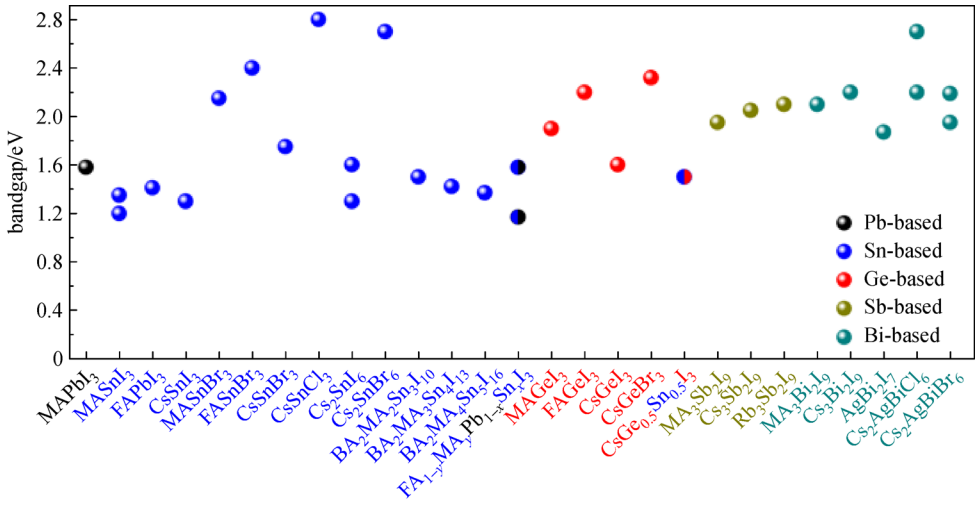

Fig. 9 Bandgaps of different multi-dimensional perovskite materials [113]

composition from the ultraviolet region all the way to the infrared region [10,114]. A common technique used is the modification of the halide ion used in synthesis to change the unit cell size and composition, which in turn alters the bandgap range from 1.1 to 3.4 eV [10,104,106,115–117]. Considering ABX_3 structure, for X = Cl, the bandgap can be tuned to 3.4 eV, and that value decreases to 2.3 eV for X = Br and 1.55 eV for X = I. Thus, there is an increase in the bandgap when the halide anion X decreases in size as seen in Fig. 10, which is in agreement with Vegard's law too [10,104,119].

Moreover, changing the cation A can have similar effects on the bandgap, as highlighted in Fig. 11. A study led by Eperon et al. was conducted on mixed halide perovskites to measure the change in bandgap range with the size of the cation A [116]. The perovskites compared were $MAPbI_3$ and formamidinium lead bromide-iodide ($FAPbI_xBr_{3-x}$). Smaller bandgaps and various absorption ranges were recorded at different x values for $FAPbI_xBr_{3-x}$. The bandgap value obtained at $x = 3$ for example was 1.48 eV compared to 1.57 eV of pure $MAPbI_3$. On the other hand, the smaller bandgap of $FAPbI_3$ provided a wider absorption of the spectrum around 840 nm due to a crystalline structure change from cubic for $x < 0.5$ to tetragonal for $x > 0.7$. The change in cationic radius resulted in the expansion of the perovskite lattice, which in turn decreased the bandgap range [104,116].

Low-dimensional perovskites have been attracting a lot attention lately due to their unique qualities, and similarly to 3D perovskite, their bandgaps and absorption ranges are highly dependent on their geometric size and structures [121]. When tested at low temperatures, the bandgaps of low-dimensional perovskites appear as clear singular step-like peaks on the absorption spectrum [122], and that is due to the fact that light absorption behaves in a step-like

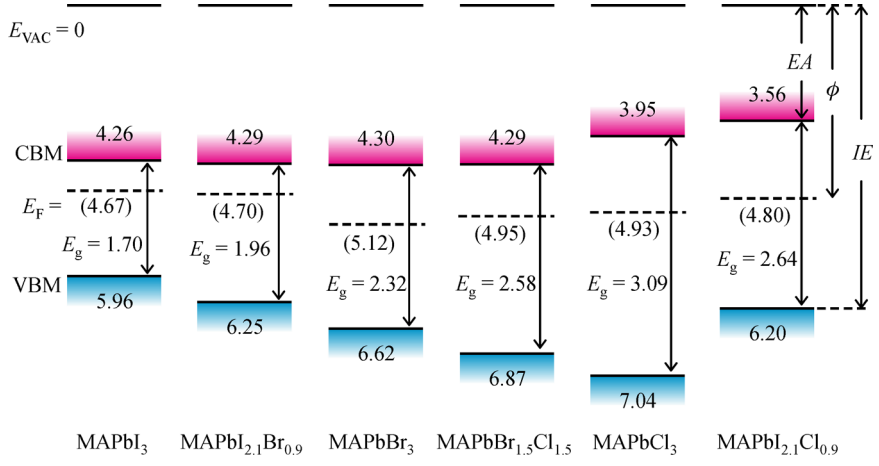

Fig. 10 Several perovskite films with varying X-site halide anion and their respective bandgaps and Fermi levels. Reprinted with permission from Ref. [118], Copyright 2018, Wiley

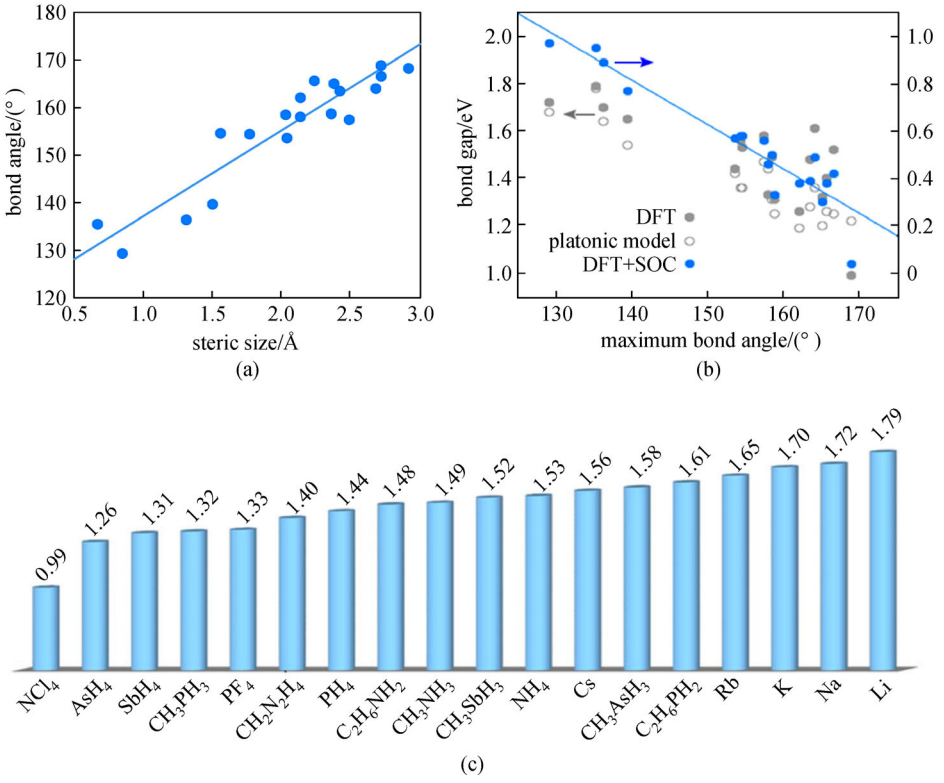

Fig. 11 Correlation between different A site cations and their (a) steric sizes, (b) bond angles and (c) bandgap values. Reprinted with permission from Ref. [120], Copyright 2014, Springer Nature

manner near the bandgaps [31,123]. Figure 12 shows several examples of 2D material and their respective bandgaps.

2D and quasi-2D perovskites are highly tunable and present unique optoelectronic attributes due to their ionic bonds in the crystalline lattice and their tunable quantum well structure by substitution of their organic components [121]. Several reports have stated that it was possible to replace the X anionic site or to perform partial substitution of B halide cations in 2D structures to tune the bandgap as well [31,122,123,126,127]. Exchanging Cl with Br in the 2D structure was reported to enable tuning of the absorption range by Lanty et al., whereas Weidman et al. determined that changing the A cation site has a small impact on these properties [31,126,127]. In addition, an increase in layer numbers (*n* value in the 2D and quasi-2D structure) decreases the bandgap, which can be attributed to a weakened quantum confinement effect [31,121,128]. The tunability range of 2D and quasi-2D halide perovskites has been shown to be close to 1.5 eV in magnitude, going from approximately 2.2 to 3.7 eV [31,121].

Molecular substitution is also a bandgap tuning technique used for 1D and 0D halide perovskites. In the case of nanowires specifically, their diameter is a defining factor in terms of bandgap energy and absorption wavelength [129], whereas exchanging Cl, Br and I halide cations at the X site proved that wide range tuning was possible for both 1D and 0D perovskites, providing good absorbance over the visible spectrum and near the infrared region [130]. Tuning the A site is another option, with FA-based 0D perovskites showing higher absorption and wider bandgaps in comparison to MA-based 0D perovskites [130]. In the case of $CsPbI_3$ quantum dots, their cubic phase provides extensive absorption and a bandgap around 1.73 eV [2,130,131]. Their main disadvantage is their instability at room temperature where their cubic structure transforms to orthorhombic. This was mitigated by partial substitution of I with Br, but the impact on bandgap was unfavorable as the new material caused extensive recombination at the interface of the hole transport layer and the perovskite film, leading to a reduction in performance [2,132,133].

2.2.2 Carrier dynamics

The high-charge carrier mobilities and low recombination rates were observed early on in metal halide perovskite research [134]. Further reduction of unwanted recombination has been a driving force in advancement of perovskite devices. There are three main modes of recombination in perovskites: trap-assisted, bimolecular, and Auger, and they are shown in Fig. 13.

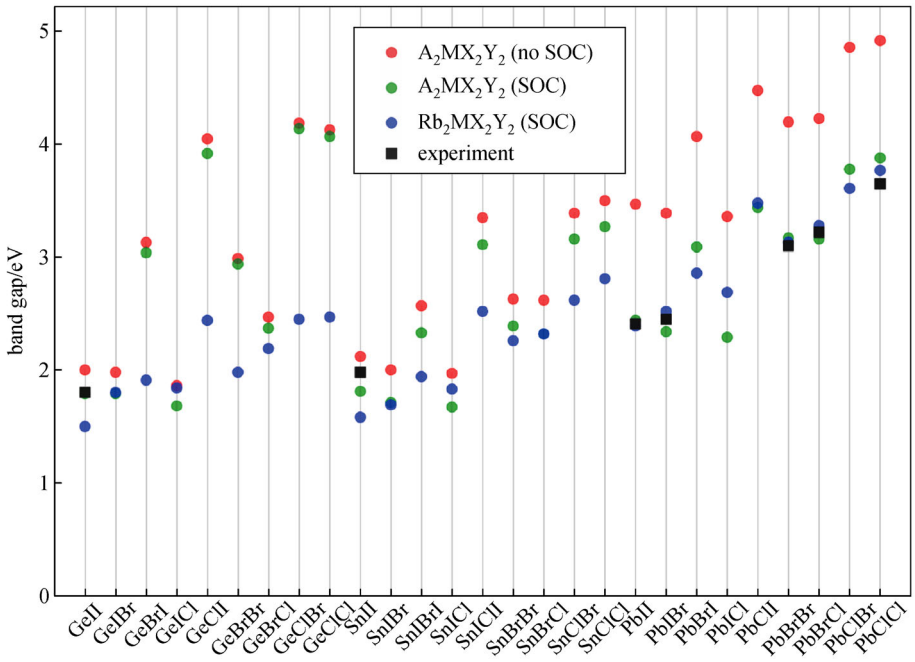

Fig. 12 Different bandgap values for 2D perovskites with spin-orbit coupling (SOC) or without (no SOC). The name representation show the metal atom first with the in-plane and axial halogens [15,124,125]

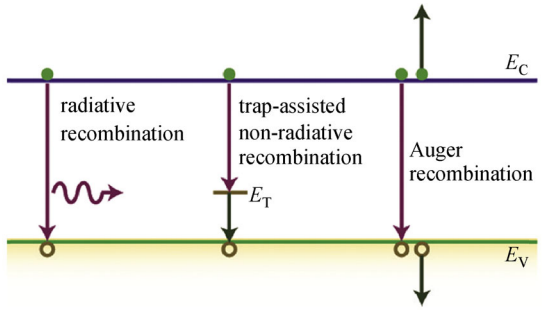

Fig. 13 Diagram showing recombination mechanisms in halide perovskite. Seen from left to right: bimolecular, a radiative process where an electron from the conduction band (CB) and hole from the valance band (VB) combine to produce a photon. Trap-assisted recombination, a monomolecular, non-radiative process where a carrier moves to a defect induced localized energy level between the VB and CB. Auger recombination, a non-radiative process where a carrier transmits its energy to a carrier of the same type allowing it to recombine. Reprinted with permission from Ref. [135], Copyright 2018, Woodhead Publishing

Bimolecular recombination is present in any direct bandgap semiconductor and is preferred to the other forms of recombination because it is radiative. This is favorable as it contributes to and increases photon density within the material, resulting in a higher operating voltage for perovskite devices [10,136]. Bimolecular recombination rates in 3D perovskites are orders of magnitudes smaller than predictions from Langevin theory [137,138]. The probability of radiative recombination, and thus the rate, can be increased by the confinement of electrons and holes, a factor strongly influenced by the dimension of the perovskite structure [105]. The other two types of recombination are non-radiative and are generally considered loss mechanisms.

Trap-assisted recombination is a form of non-radiative recombination facilitated by a trap site such as an impurity or a crystal defect [137]. Trap state density has been found to be higher at the surface of 3D perovskite crystals than in the bulk [137,139,140]. This trend is thought to continue in molecular 2D perovskites and nanocrystals [141,142], although Freppon et al. has observed nanocrystals that appear to have no trap assisted recombination [143]. Trap states can lead to losses but not all trap states are created equal. Shallow traps states are preferential formed in lead halide perovskites [144]. These trap states exist near the conduction or valance band and are less detrimental to performance than deeper trap states. Carriers trapped in shallow states can be easily freed by a small amount of energy, while deep trap states facilitate easier recombination and thus greater losses [10,106,145].

The other form of non-radiative recombination is the Auger recombination, which becomes the dominate mode of recombination at very high carrier concentrations. Making this type of recombination much more common in perovskite LEDs than other devices like solar cells [138,143]. As such, this process is application based and only indirectly related to dimensionality.

How the electrons and holes move within a semiconductor

will have a significant impact on how they recombine. In materials with high dielectric constants, such as in Si and GaAs, excitons with low binding energies around 10 meV are formed [10,146]. With the available thermal energy of ~26 meV at room temperature, these excitons can be easily dissociated to generate free charge carriers in high efficiency devices. Studies have shown that 3D perovskites also have a similarly high dielectric constant [10,139,146] and it correlates well with reports of exciton binding energy for these materials being below 26 meV [147,148]. This suggests that at room temperature excitons in 3D perovskite dissociate into electrons and holes, behaving like more conventional semiconductors. Although some have proposed that the excess electrons and holes form large polarons. A polaron occurs when an electron or hole is trapped by charges in the crystal lattice and that trapped charge deforms the surrounding lattice. This deformation extends across multiple unit cells in the case of a large polaron, making it behave like an electron or hole but with a larger effective mass and reduced scattering [149,150].

While 3D perovskites may have low exciton binding energies, this is not always the case for lowdimensional perovskites, with 2D and low-dimensional perovskites displaying binding energies in the hundreds of meVs [151–153]. This increase in binding energy could be due to the increased confinement of electron-hole pairs. The organic ligands incorporated into low-dimensional perovskites have low dielectric constants, and relatively weak van-der-Waals interactions, and these effects work to further confine the excitons [9,17,152]. Liu et al. compared a variety of characteristics along the interior of the crystal and its edges [77]. The results showed that the organic cationic compounds of low-dimensional perovskites behave like insulators, stationed between inorganic conducting layers. The confinement of the carriers led to longer charge carrier lifetime, higher photocurrent, and increased carrier mobility within the crystals [153,154]. Shorter average carrier lifetimes are indicative of more non-radiative recombination [155,156]. An extension of carrier lifetime suggests that carriers are recombining at trap sites. This may be due to passivation of surface trap sites by the organic ligands [141,142]. Another factor increasing lifetime is the restriction of carrier movement. As the dimensionality of the perovskite decreases there will be fewer free-excitons and more self-trapped excitons [2]. These self-trapping excitons become trapped by other charges in the lattice and warp the lattice around them. This description is similar to the large polaron described earlier, but unlike the extensive lattice distortion carriers may impact on 3D perovskite, the distortion caused by excitons on low-dimensional perovskite does not extend far beyond the structural site. This makes the self-trapping exciton analogs a small polaron, a carrier which is less mobile than a free exciton or large polaron. The reduction in mobility caused by this self-trapping is accompanied by an increase in carrier lifetime [149].

Low-dimensional perovskites synthesized without organic ligands possess different carrier properties. Yang and Han compared perovskite nanoplatelets with and without organic ligands, showing that ligand free nanoplatelets had reduced carrier lifetimes. This is attributed to the lack of surface passivation and a reduction in long lived, self-trapping carriers [157]. Devices built with ligand free perovskite nanoplatelets demonstrated a large amount of electron-hole separation, suggesting lower exciton binding energies than low-dimensional perovskites with organic components [158].

The properties of the organic component incorporated into low-dimensional perovskite has a substantial effect on the material's transport properties. There have been studies working on incorporating functional organic molecules into low-dimensional perovskites to alter the properties of the material [159–161]. Gélvez-Rueda et al. were able to improve charge separation in perovskite nanoplatelets by replacing non-functionalized organic ligands with perylene diimide, which is an electron acceptor [161]. The ability to tailor perovskites of different dimensions makes them applicable for use in a variety of devices.

2.2.3 Ion migration

Ion migration in metal halide perovskites is a topic of interest due to its photoactive nature and for the roll it may play in phenomena such as switchable photovoltaics [162,163], a photo-induced giant electric constant [164], photo-induced poling effect [165], self-healing [166,167], photo-induced phase separation [168] as well as a degradation process which impacts devices in the long-term [169,170]. Like the movement of carriers, the movement of ions within perovskites is affected by the dimensionality of the material. Ion migration can refer to the movement of ions intrinsic to the perovskite (e.g., Pb^{2+}, MA^{+}, I^{-}, Br^{-}) within the perovskite structure as well as extrinsic ions (e.g., Li^{+}, Na^{+}) from other layers of a device moving through the perovskite [171]. This movement can be prompted by electric fields throughout a device, or localized electric fields created by trapped carriers [169,172]. The migration of ions in perovskites is thought to be mediated by vacancy point defects in the material [169,173], where the migrating ion hops from its lattice position to a nearby vacant one. A material with fewer defects will experience less ion migration. Thermally activated defects that are intrinsic to the crystal's chemical makeup can be expected in a crystal above 0 K, but additional defects can be introduced in the fabrication of perovskites. The production method of the material will impact the defect density of the perovskite. For example, 3D perovskites with small grain sizes experience an increase in ion migration [174]. This can be explained by

channels for ion migration forming along grain boundaries due to the increased defect density in these areas and having decreased grain size corresponds to an increase in grain boundaries [152,169,175].

This is different from what occurs in low-dimensional perovskites that incorporate organic ligands. Due to the passivation of surface defects by the organic component ion migration is less favorable on these surfaces [175]. This is one reason 2D perovskites experience less ion migration than 3D perovskite. Cho et al. compared 2D and quasi-2D perovskites of different dimensionality and showed that reduction in dimensionality reduces ion migration [173]. The suppression of migration by organic ligands can also be seen with perovskite nanocrystals. Some ligand-free nanocrystals exhibit ion migration between crystals, while nanocrystals with organic ligands showed no signs of ion migration [152,172]. However, the effects of surface passivation on ion migration are not unique to organic ligands: Lamberti et al. used laser ablation synthesis to produce ligand-free perovskite nano crystals that did not exhibit ion migration [176]. This shows that the reduction in ion migration with dimensionality depends on the production methods used to create the low-dimensional perovskite structures.

3 Applications

3.1 Photodetectors

Photodetectors convert incident light into current or voltage outputs [4,177–179]. They are one of the more commonly used semiconductor devices, used in many applications such as biomedical imaging, environmental monitoring, spectroscopy, fiber-optic communication, and astronomy [4,178,180]. However, typical inorganic photodetectors are relatively expensive requiring high temperature and pressure to be produced and must be operated at low temperatures to detect low levels of light [34,181]. Furthermore, they are mechanically rigid [179,180], and do not meet the demand of large-area applications [180] and wearable electronics [179]. Organic photodetectors, on the other hand, offer advantages with respect to cost, weight and flexibility [180] however suffer from poor charge-carrier mobilities [34]. It is evident that novel device materials and architectures are needed to drive technological advancements in the realm of photodetectors [4].

Using direct bandgap metal halide perovskites in photodetectors provides the benefits of both organic and inorganic semiconductors: solution processability, low-temperature synthesis, bandgap tunability, long charge carrier diffusion lengths, and high absorption coefficients [4,177,179] (up to ~10^5 cm^{-1} in the UV-visible range) [34,182]. Moreover, photodetectors employing halide perovskites exhibit high sensitivity and fast response because of their unprecedented low recombination rates [179,183,184]. Furthermore, the material set and dimensionality of the perovskite can be customized to make application-specific photodetectors with desirable performance metrics [4]. Metal halide perovskites are ideal for low-cost, high-performance photodetection [34,179] and have thus gained significant attention in recent years [2–4,6,179].

Photodetectors are typically evaluated using several important figures of merit such as high responsivity (R), external quantum efficiency (EQE), specific detectivity (D^*), and gain (G) [179,180] narrow spectral selectivity, and short response time [180,181]. Responsivity (R) represents the amount of current generated per unit of power illumination at a specific wavelength radiation and is defined in Eq. (2).

$$R = \frac{I_{\text{light}} - I_{\text{dark}}}{P_{hv}}, \tag{2}$$

where I_{light} is the photocurrent, I_{dark} is the dark current and P_{hv} is the incident light intensity [185,186].

The external quantum efficiency (EQE) is the ratio of the number of charge carriers collected to the number of incident photons and is defined in Eq. (3).

$$\text{EQE} = \frac{Rhc}{e\lambda}, \tag{3}$$

where R is the responsivity, h is Planck's constant, c is the speed of light, e is the electron charge, and λ is the wavelength of incident light [185,186,191].

The specific detectivity (D^*) is an important figure of merit for photodetectors expressed in $\text{cm}\cdot\text{Hz}^{0.5}\cdot\text{W}^{-1}$ (Jones) [11] and is defined in Eq. (4).

$$D^* = \frac{\sqrt{AB}}{\text{NEP}} = \frac{e\lambda\sqrt{A}(\text{EQE})}{hci_{\text{noise}}}, \tag{4}$$

where A is the active area of the photodetector, B is the operation bandwidth, NEP is the noise equivalent power, i_{noise} is the noise current [186,191].

Gain (G) is another important parameter of photodetectors, which represents the number of carriers that can be produced in an external circuit per incident light illumination. It is described by the following formula:

$$G = \frac{\tau_{\text{h}}}{\tau_{\text{t}}} = \frac{\tau_{\text{h}}\mu V}{d}, \tag{5}$$

where τ_{h} is the lifetime of the holes, τ_{t} is the transportation time of carriers to electrodes, d is the device thickness, μ is the carrier mobility, and V is the applied bias [185].

Response time reflects the response speed to incident light. It is characterized by a rise time (the time to rise from 10% to 90% of the maximum photocurrent) and decay time (time to decay from 90% to 10% of the maximum photocurrent) [179].

According to the spatial layout of the perovskite and electrodes, vertical and lateral structure perovskite photodetectors can be created [177,180]. A lateral-structure photodetector, such as a photoconductor or phototransistor, has a slower response than a vertical-structure photodetector but can achieve EQEs over 100% and consequently high gain [177,180]. 3D perovskite has been used extensively to fabricate photoconductor devices [4,57,182,184–187]. A perovskite photoconductor has an absorbing layer between two transverse metal electrodes [179]. In a perovskite photoconductor, the photosensitive layer produces a carrier bias when illuminated, which is separated at a set voltage and extracted at the electrodes [179]. Perovskite photoconductors are easy to produce and have great potential in flexible electronic devices [179]. In fact, the first perovskite photoconductor was created by Hu et al. by depositing a $MAPbI_3$ film on a flexible substrate using a one-step solution processing method [188]. This photoconductor was good for a broadband wavelength, with a responsivity of 3.49 A/W under UV light and 0.0367 A/W under visible light [188]. Lateral perovskite photodetectors have simultaneous high detection capability and signal magnification capabilities [180]. Zeng et al. recently recorded high performance for all figures of merit by employing a confined growth strategy to create a 3D perovskite ($CsPbBr_3$) photoconductor. The finished device demonstrated a responsivity of 216 A/W and ultrashort response time (<5 μs), better than all the $CsPbBr_3$ photoconductors, along with a record detectivity of 7.55×10^{13} Jones [187]. More recently, Hasan et al. used a blade coating technique to create highly oriented mm-sized crystal grains in a stable lateral photoconductor [57]. This photoconductor exhibited an order of magnitude improvement in responsivity over previously reported 3D perovskite polycrystalline thin films with channel lengths over 100 μm [57].

The photodiode is an example of a vertical-structure photodetector that can obtain a fast response [177,179,180] and high detectivity because of the small electrode spacing with a short carrier transit length, as shown in Fig. 14 [177,180]. The difference between lateral-structure photodetectors and vertical-structure photodetectors is shown in Fig. 14 [189].

Vertical-structure photodetectors can be further subcategorized into regular (n-i-p) and inverted (p-i-n) types. In these types of photodetectors, the active layer (perovskite) is sandwiched between a hole-transporting layer (HTL) and an electron-transporting layer (ETL). Incorporating these extra layers increases the possibility for defects at the interface, which increases the recombination of charge carriers. As such, much effort has been made into reducing the traps at the interface through interfacial and band alignment engineering [6,8,180].

Regular n-i-p perovskite photodetectors consist of a transparent n-type layer atop a light harvesting layer (perovskite) followed by a p-type contact layer [180]. As mentioned above, these photodetectors can exhibit high detectivity. By engineering the ETL and HTL, Fang and Huang reported a low noise 3D perovskite ($MAPbX_3$, where X = Cl, I or Br) photodetector that can respond to weak light at around 0.6 pW/cm^2 [185].

Inverted p-i-n perovskite photodetectors typically consist of a highly doped transparent p-type layer above an absorbing layer (perovskite), followed by a highly doped n-type layer [180]. Recently, Dou et al. created an inverted 3D perovskite ($MAPbI_{3-x}Cl_x$) photodetector with a detectivity approaching 10^{14} Jones between 350 and 750 nm at 100 mV [186]. The performance metrics of photodetectors with different dimensionalities are shown in Table 2.

More recently, there has been research into single-crystal perovskite vertical photodetectors [180,192]. Single-crystal based devices are anticipated to have superior performance [182,192] and improved stability [6] resulting from the lack of grain boundaries. Fang et al. created highly narrowband mixed perovskite single-crystal photodetectors ($MAPbBr_{3-x}Cl_x$ and $MAPbI_{3-x}Br_x$) by tuning the halide composition, changing the absorption edge continuously from blue to red [182]. In addition, Geng et al. reported a rise time as fast as 520 ns, comparable to

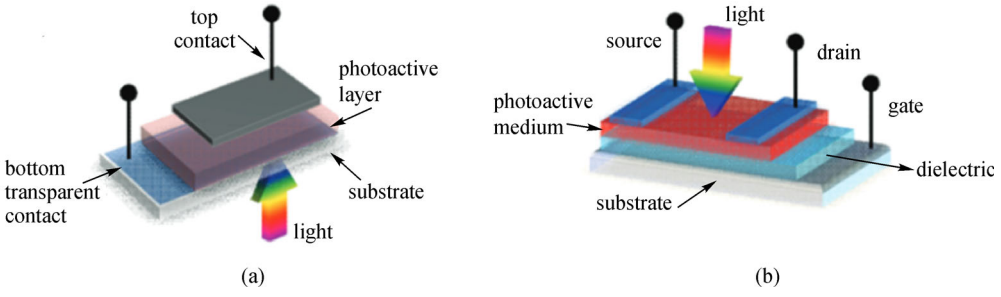

Fig. 14 Diagram demonstrating difference between (a) vertical-structure and (b) lateral-structure photodetectors. Vertical-structure photodetectors possess a transparent incident light window at the bottom. In contrast, lateral-structure photodetectors have an incident light window on top. Reprinted with permission from Ref. [189], Copyright 2013, Wiley

single crystal germanium photodetectors, by integrating a single-crystal 3D perovskite with a Si wafer [184]. Moreover, Cheng et al. used a novel two-step temperature method to make high-quality (defect density of ~7.9 × 10^9 cm^{-3}, comparable with the best quality crystals of metal halide perovskites reported) UV photodetectors with high performance using $MAPbCl_3$ single crystals [192].

2D perovskite materials have garnered interest in photodetectors because of their strong size effects and sizable band gaps [179]. Liu et al. created 2D perovskite ($MAPbI_3$) nanocrystals with unit cell thickness (~1.3 nm) for use in photodetectors by combining a solution processing method with a vapor-phase conversion method [197]. The photodetector showed a responsivity of 22 A/W and fast rise and decay times of less than 20 and 40 ms, respectively [197]. The development of 2D perovskite photodetectors has been hindered by the inability to grow large area and shape-controlled single crystals [4]. Using a new crystallization method, Liu and colleagues grew well-defined inch-sized $(PEA)_2PbI_4$ 2D perovskite single crystals [53]. In this work, the quality of the crystals was defined by their nucleation and growth. The single crystals were preferentially grown at the interface of the solution and air, combining the well-known inverse temperature crystallization method with surface tension control. Using this method, a photo responsivity of 139.6 A/W, an EQE of 37719.6%, a detectivity of 1.89 × 10^{15} Jones and a fast response speed (T_{rise} = 21 μs, T_{decay} = 37 μs) was achieved. Furthermore, the low defect density resulted in an ultralow noise current, translating into high detectivity. This work represented progress into the development of filterless, color-selective and narrowband photodetection [4,53]. Recently, Qian et al. replaced the Pb with Sn in 2D perovskite and created a flexible $(PEA)_2SnI_4$ perovskite photoconductor using a one-step solution processing method [20]. This extremely durable device achieved good responsivity (16 A/W) and detectivity (1.92 × 10^{11} Jones under 470 nm illumination) and effectively mimics the short-term plasticity of biological synapses [20].

Although both 3D and 2D perovskite photodetectors have attracted significant attention, 1D perovskite photodetectors may offer significant advantages over their thin-film counterparts [183]. The inherent reduced density of grain boundaries permits smoother charge flow, potentially leading to increased performance [179,183]. Furthermore, 1D perovskites such as nanowires exhibit strong flexibility, enabling the realization of flexible photodetectors on polymer substrates. There is also evidence that these 1D nanowires perform comparably or even better than their large single crystal counterparts because of their low defect levels [183]. First, using a simple slip-coating method, Horváth et al. produced $MAPbI_3$ nanowires with lengths up to 10 μm that exhibited responsivities up to 5 mA/W, comparable with the 2D devices at the time [83].

1D perovskite nanowires possess a small volume to surface area ratio, which leads to enhanced degradation by moisture and light [180,183]. Surface passivation may be needed to maintain the performance of these 1D photodetectors over time. To that end, Gao et al. used a one-step self-assembly method to synthesize a $CH_3NH_3PbI_3$ array of nanowires and treated it by soaking it in oleic acid (OA), which remarkably enhanced the electrical characteristics as well as the device stability. The devices exhibited submilisecond response time, as well as a detectivity of 2 × 10^{13} Jones, five-times better than Si-based commercial photodetectors (4 × 10^{12} Jones). Finally, after one-month storage in air, the photocurrent degrades to 94% for the OA passivated device, in comparison to 28% for the untreated control [183].

The excitons in 0D perovskites are confined in all three dimensions, which leads to unique optoelectronic properties because their energy band can be tuned by changing their size and shape [179]. Furthermore, their large surface area-to-volume ratio promotes light detection, which is favorable for photodetection [179]. 0D perovskite nanocrystals with interesting optoelectronic properties (e.g., $CsPbBr_3$) are frequently combined with other materials to create heterojunction photodetectors [179,200,202]. For

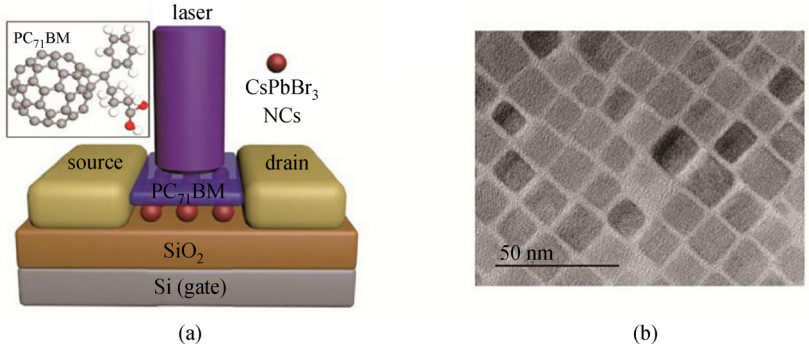

Fig. 15 (a) Architectural device schematic showing the structure of the bulk heterojunction photodetector. The bottoms substrate consists of an Si gate, an SiO_2 gate dielectric, and Au source/drain electrodes. The active layer is a heterojunction of perovskite nanocrystals and $PC_{71}BM$). The inset depicts the chemical structure of $PC_{71}BM$. (b) HRTEM image of the $CsPbBr_3$ nanocrystals, scale 50 nm. Reprinted with permission from Ref. [200], Copyright 2017, ACS Publications

example, Li et al. created an efficient bulk heterojunction photodetector by incorporating $PC_{71}BM$ ([6,6]-phenyl C_{71} butyric acid methyl ester) with $CsPbBr_3$ nanocrystals as seen in Fig. 15(a). The photodetector is obtained via simple spin-coating therefore this work provides a framework to make high performance photodetectors that combine perovskite and organic matter [200]. Figure 15(b) shows the high-resolution transmission electron microscopy (HRTEM) image of the $CsPbBr_3$ nanocrystals, which have a highly crystalline and cubic structure and an average size of approximately 13 nm [200].

Jang et al. also reported using a novel ultrasound-synthesis method to make high-sensitivity photodetectors using perovskite nanocrystals with a wide range of compositions [203]. In this work, the photodetectors are created by homogeneously spin coating the uniform nanocrystals on thermally oxidized large-area SiO_2 substrates. In general, there is still urgent work needed into low toxicity and high stability perovskites, large-scale photodetector arrays on flexible substrates, and integration of photodetector materials with other electronic components [4]. Table 2 summarizes the different dimensionalities of the perovskites mentioned above, along with the relevant figures of merit describing each device.

3.2 Solar cells

Perovskite solar cells (PSCs) have been quite the hot topic in the field of renewable energy in the last decade, and that is due to their proficiency in converting the sun's energy into clean electricity and the progress achieved in such a short time, from 3.8% efficiency in 2009 [40] to 25.2% ten years later [73,204]. In solar cells, this process is known as photovoltaic conversion, where photons having high enough energy travel from the valence band to the conduction band after photoexcitation. The minimal photon energy required is noted as E_g, which can be found using the following equation:

$$E_g = h\upsilon = \frac{hc}{\lambda}, \tag{6}$$

where E_g represents the energy, h is Planck's constant, υ is the frequency, c is the speed of light, and λ is the wavelength [205].

While E_g determines the highest potential value for the extraction of a photocurrent, the bandgap is also a determining factor to attain the highest possible PCE and short-circuit photocurrent (J_{sc}) by the device when exposed to sunlight. In other terms, considering the Shockley–

Table 2 Perovskite photodetectors, their dimensionalities, and relevant figures of merit

perovskite/dimensionality	device	$R/(A\cdot W^{-1})$	EQE/%	D^*/Jones	response time (rise/fall time)	Ref.
$MAPbI_3$/3D	photoconductor	3.49	1190	–	< 0.1 s	[188]
	photoconductor	164.2	~2×10^4	–	–	[57]
	photodiode	2.71	–	3.4×10^{13}	–	[190]
	photoconductor	219	4.1×10^4	3.1×10^{12}	–	[191]
$MAPbCl_3$/3D	photoconductor	3.73	1115	$> 9 \times 10^{11}$	130 ns	[192]
$MAPbBr_{3-x}I_x$/3D	photoconductor	0.055	–	–	< 20 μs	[193]
$MAPbX_3$, (where X = Cl, I or Br)/3D	photodiode	0.21	93	7.4×10^{12}	< 500 ns	[185]
$MAPbI_{3-x}Cl_x$/3D	photodiode	–	80	8×10^{13}	~ 600 ns	[186]
$MAPbBr_x$/3D*	photodiode	–	3	2×10^{10}	–	[182]
$MAPbBr_3$/3D	photodiode	0.0136	–	5.9×10^{10}	520 ns / 2435 ns	[184]
$CsPbBr_3$/3D	photoconductor	216	17.64	7.55×10^{13}	< 5 μs	[187]
$(PEA)_2PbI_4$/2D	photoconductor	139.6	37719.6	1.89×10^{15}	21 μs / 37 μs	[53]
$(PEA)_2SnI_4$	photoconductor	~16	–	1.92×10^{11}	0.63 s / 3.6 s	[20]
$CsPbBr_3$/2D**	photoconductor	10.85	3390	3.06×10^{13}	44 μs / 390 μs	[194]
$MAPbI_3$/2D	photodiode	0.036	–	–	320 ms / 330 ms	[195]
	photoconductor	4.95	–	2×10^{13}	< 0.1 ms	[183]
	photoconductor	0.0052	–	–	500 μs	[196]
	photoconductor	22	–	–	< 20 ms / < 40 ms	[197]
$MAPbI_3$/1D	photoconductor	4.95	–	2×10^{13}	< 0.1 ms	[183]
	photoconductor	0.005	0.4	–	< 0.5 ms	[83]
$MAPbI_3$/1D	photodiode	1.32	–	2.5×10^{12}	0.3 ms	[198]
$CsPbBr_3$/0D	photoconductor	0.02092	16.69	4.56×10^8	0.2 ms / 1.2 ms	[199]
	photodiode	1.72	530	1.76×10^7	~0.09 ms / ~ 0.1 ms	[200]
$CsPbBr_3$/0D***	photoconductor	–	–	–	24 ms / 29 ms	[201]

Notes: * This device exhibited highly narrowband detection capabilities. ** This device was integrated into a heterojunction with polymerphenyl-C61-butyric acid methyl ester (PCBM). *** This device exhibited a good on/off current ratio of 10^5.

Queisser limit [206], a single junction photovoltaic device with an optimal bandgap of 1.34 eV can reach a maximum theoretical value of 33% in terms of total power extracted from the solar spectrum [205,206].

PSCs are characterized using the standardized method of illumination with the AM1.5G spectrum at 1000 W/m^2 intensity. The current values are recorded as a function of applied voltage, and current–voltage (J–V) curves are drawn, as depicted in Fig. 16.

Voltage sweeps can be done in the forward and reverse directions. Three parameters are noted from the findings: the short-circuit current obtained at zero applied potential, the open-circuit voltage (V_{oc}) needed to push the current to zero, and the fill factor (FF) [205,208]. These variables are used to determine the solar to power conversion efficiency of a PV device. By measuring the applied potential (V) against the current density (J), the PCE of PV device can be obtained using the following equation:

$$\mathrm{PCE} = \frac{J_{\max} V_{\max}}{P_{\mathrm{in}}} = \frac{J_{\mathrm{sc}} V_{\mathrm{oc}} \mathrm{FF}}{P_{\mathrm{in}}}, \tag{7}$$

where $J_{\max}$ and $V_{\max}$ are the maximum current and voltage values respectively, and P_{in} is the input power. Therefore, the PCE of a PV device can be increased by changing these variables. The capture of more photons and the reduction of the recombination losses will lead to an increase in J_{sc} [205,206,208,209].

Nowadays, it is widely agreed on that PSCs function similarly to p-i-n and n-i-p solar cells as shown in Fig. 17.

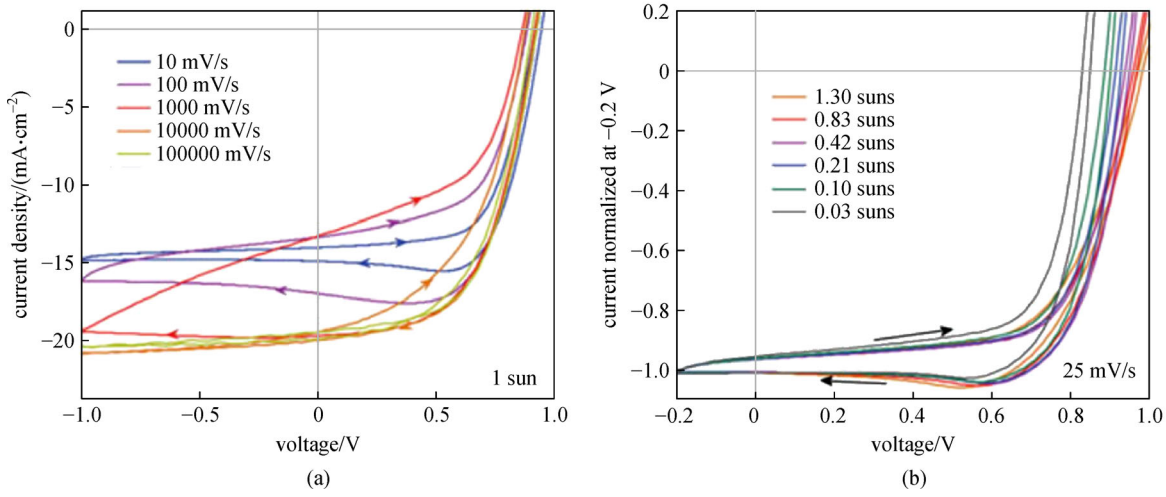

Fig. 16 J–V characteristic curves of PSC using different (a) scanning speeds and (b) illumination intensities [207]

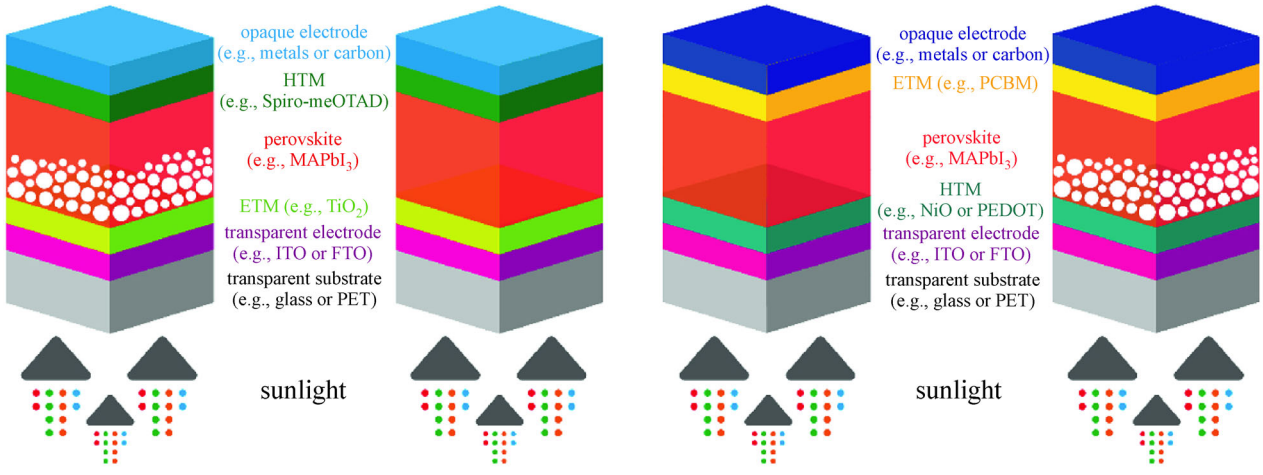

Fig. 17 p-i-n and n-i-p architectures used in the production of perovskite solar cells. Reprinted with permission from Ref. [10], Copyright 2020, Springer Nature

Perovskite, an intrinsic light absorber, is placed in both architectures between two selective contacts, ETL and HTL [6,8,180,209]. Two electrodes are placed on each end as well to allow the current flow. Higher PCE, approximately 22.1%, have been reported for devices with n-i-p structures [210]. There are different materials to choose from for the HTL and ETL, highlighted in Fig. 18. Even though the choice and treatment of these layers can help limit recombination losses [10,211], the selection process is mainly based on the appropriate conduction and valence band energy levels, and the bandgaps and Fermi-levels of the transport layers [212]. For this reason, the most common substances in an n-i-p structure have been Spiro-OMeTAD (p-type) as HTL and TiO_2 (n-type) as ETL [209,213,214], whereas PEDOT:PSS (p-type) and fullerene derivatives, specifically PCBM (n-type), have been constantly chosen as HTL and ETL respectively in the inverted p-i-n devices [209,215–218].

3D halide perovskites are constantly studied as there has been considerable progress in terms of PCE throughout the years [219]. A lot of work has been done tuning the 3D lattice and changing the major components to achieve the best practical efficiency for a single-junction cell [10,213,220–224]. In particular, $MAPbI_3$ has been researched extensively as a prime 3D candidate for solar cells. Zhang et al. developed a solvent coordination and anti-solvent extraction method that helps shorten conversion time in 3D $MAPbI_3$ formation from 1 h to around 10 min, all while suppressing large grain formation to achieve good porous films and device reaching 15.6% PCE [225]. A different work used methylammonium acetate (MAAc) to retard the perovskite formation reaction rather than enhance it. This approach allowed the formation of uniform perovskite films with controlled morphology due to the anionic exchange between Ac^- and I^-, and achieved 18.09% efficiency when used in a PV device [226]. Another morphology control technique was employed by Zhou et al. to improve thin film quality. Using water to induce intermediate phase formation, grain size and film morphology were manipulated under heat assisted spin coating processing (HASP). 19.12% PCE was reached in an inverted PSC, while a single junction 1.2 cm^2 area device was able to maintain 15.47% efficiency with negligible hysteresis [227]. A 20% PCE device was reported by Liu et al. using a mixture of low boiling point solvents. The solution consists of $MAPbI_3$ precursor in a mixture of ethanol and tetrahydrofuran [221]. The same precursor solution was used in another report where an inverted solar cell was made using copper thiocyanate (CuSCN) thin film as HTL. Post treating HTL with potassium thiocyanate (KSCN) boosted the short J_{sc} value from 16.71 to 19.2 mA/cm^2, which in turn increased the cell's efficiency from 11.9% to 14.9% [223]. A novel deposition technique was developed by Ye et al. labeled soft-cover deposition (SCD) method. It was used to produce a pinhole free uniform 3D $MAPbI_3$ thin film in ambient air, with a large crystal size over a 51 cm^2 area. 17.6% efficiency was reached in a 1 cm^2 with small hysteresis [228]. Different precursor solutions have been tested as well, with reports showing that 12.18% PCE can be achieved using $(FAPbI_3)_{0.85}(MAPbBr_3)_{0.15}$ films, along with a good stability and J_{sc} value of 23.14 mA/cm^2, V_{oc} of

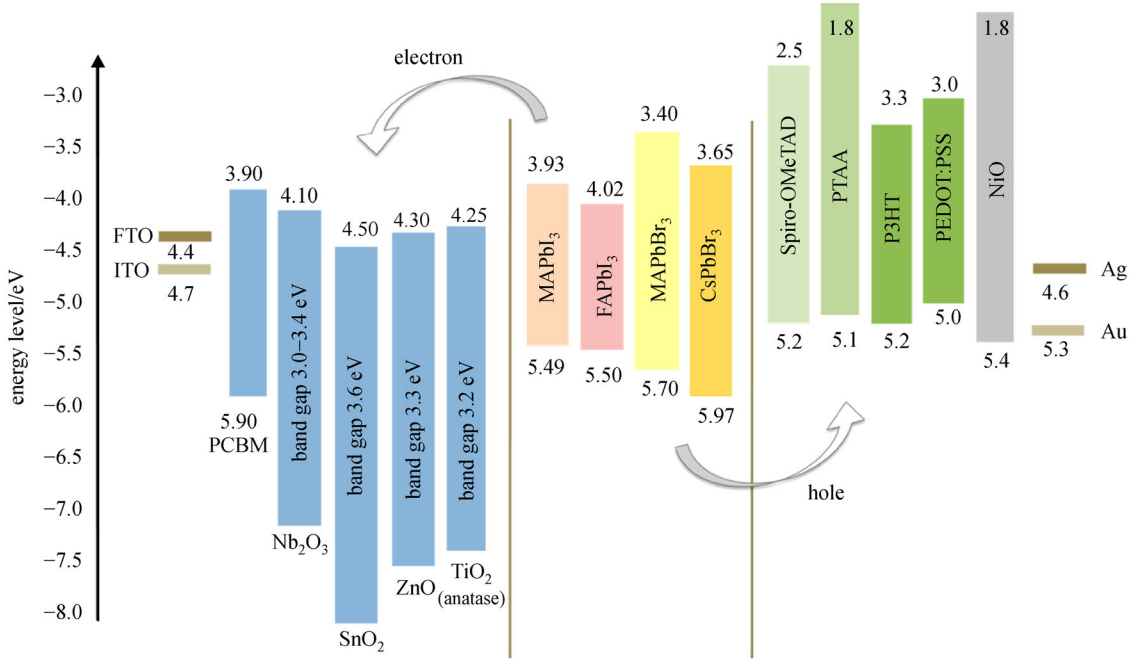

Fig. 18 Different materials used currently in the formation of perovskite solar cell devices [209]

1.03 V and FF of 51% [224], while a value of 18% PCE was seen using $MAPb(I_{0.8}Br_{0.2})_3$ film co-processed with DMSO/MABr solution [222]. On the other hand, Hao et al. tested a lead-free 3D perovskite lattice, $MASnI_3$. Homogenous nucleation and an adjustable growth rate were achieved using DMSO and NMF solvents, along with high current density of 21 mA/cm^2. A low PCE of 5.79% was reached which was attributed to the lower PV performance of lead-free alternatives, specifically low light harvesting in long wavelength region and charge recombination at the perovskite interface [229].

On the other hand, low-dimensional perovskites, especially 2D, have garnered a fair amount of attention lately due to their inherent stability and in some cases, showing clear advantages in terms of optoelectronic properties over their 3D counterparts, such as higher charge carrier effectiveness [230,231]. One of the best results reached using 2D perovskites was achieved by Zheng et al. by adding ammonium salts to $FAPbI_3$. $(C_6H_5CH_2NH_3)_2(FA)_8Pb_9I_{28}$ was formed and showed a high PCE of 17.4%, while maintaining its stability for 500 h under 80% humid conditions [70]. On the other hand, incorporating hexamethyldiamine (HDA-0.05M) into a benzylammonium 2D lattice $(BZA)_2(MA)_2Pb_3I_{10}$ improved the conductivity, efficiency as well as the surface roughness. The lattice tested did not give the best results however, with its PCE reaching 3.33% [232]. A better result was obtained testing 2D $(CMA)_2(MA)_3Pb_4I_{13}$ based solar cell which recorded a PCE of 10.66%, FF of 62.39%, J_{sc} of 16.99 mA/cm^2 and V_{oc} of 1 V [232]. Perovskite nanowires [2,233–235] and quantum dots [2,236–238] have not been researched as much as 2D sheets, but still some interesting results have been reported. Recently, a research conducted on 1D $MAPbI_3$ nanowires by Cheng et al. showed the efficiency reached about 18.83% after doping the perovskite with N-diphenylaniline (N-DPBI). The electron extraction ability and the active area coverage were also improved in the process. However, they reported that pinholes and voids were still present even after treatment and impeded performance [233]. Other reports showed that 12.96%, 9.66% and 10.46% PCE were achieved with lead-free alternatives, namely $CsSnI_3$, $CsSnCl_3$ and $CsSnBr_3$ respectively [86]. In the case of perovskite quantum dots, a record high PCE of 6.54% in 2011 made them a hot topic for research in the field, as they have shown tunable bandgaps and sensitive across a broad absorption spectrum [239,240]. Their instability under high temperature conditions however remains an issue, with partial substitution somewhat helping to solve the problem at the expense of the bandgap as discussed earlier [133,241]. Sanehira et al. have attempted to solve this issue and recorded a 10% PCE value by purifying the perovskite with methyl acetate anti-solvent. Additional FAI coating treatment boosted the PCE to 13.43% [237].

Although 3D materials have shown the highest efficiencies thus far, all perovskite structures have shown improvements over time and will surely continue to improve. Some additional halide perovskite compositions of different dimensionality are listed in Table 3.

4 Conclusions and perspective

To summarize, metal halide perovskites are currently one of the most researched materials due to their favorable electrical and structural properties. From long diffusion lengths to wide absorption ranges and tunable bandgaps, these materials have shown that they can be ideal candidates for the next generation of optoelectronic applications. Their most interesting feature is the ability to tune their unique optical and electrical properties by changing their dimensionality and shape while using the same basic precursors. Their tunability provides a plethora of possible combinations and adjustments still uncovered for future applications. Each dimension has its unique structural and electrical properties, and through extensive research, and constant development in the last decade, 3D perovskite solar cells reached more than 25% power conversion efficiency in a relatively short time. Even though 3D perovskites have shown the most promise in terms of electrical proficiency, low-dimensional perovskites have proven to be much more stable over time, and more environmentally friendly. The development of perovskites is far from over, and dimensional engineering might be one of the main promising approaches going forward. Here are some key areas that need further investigation before metal halide perovskites can be fully adopted by the industry:

1) We still do not have enough knowledge of the fundamentals behind the kinetics and dynamics of metal halide perovskites, let alone their different dimensional properties. Further research into the rudimental properties of each dimension will facilitate and properly guide future work toward the production of better materials and applications.

2) 3D perovskite materials have shown great promise in terms of photoelectrical capabilities in different applications. However, with their inherent stability and toxicity issues, especially with lead-based perovskites, it is vital to find environmentally friendly, stable alternatives. By altering the chemical composition using different compounds, novel halide perovskites can be obtained having favorable reaction to different stimulants such as heat, oxygen, and moisture.

3) On the other hand, low-dimensional perovskites have had the edge in terms of stability and coverage area in comparison to 3D, however they have not been able to reach similar heights when it comes to electrical capabilities. Uncovering the core principles relating their unique shapes to the optoelectronic properties can lead to a better understanding of how to maximize their potential and reach higher efficiencies similar to 3D materials.

Table 3 Examples of different halide perovskite-based devices and their respective electrical properties

halide perovskite	J_{sc}/(mA·cm^{-2})	V_{oc}/V	FF/%	PCE/%	notes	Ref.
$MAPbIBr_2$ (3D)	23.58	0.891	60.8	12.79	forward scan	[220]
$MAPbIBr_2$ (3D)	23.852	0.891	71.6	15.237	reverse scan	[220]
$MAPbICl_2$ (3D)	18.98	0.82	52.98	9.3	DMF solvent/FS	[242]
$MAPbI_3$ (3D)	20.62	1.04	69	14.8	low purity PbI_2 + MAI in DMF/HCl	[243]
$MAPbI_3$ (3D)	22.48	1.04	70	16.4	enhanced crystallization using methanol	[244]
$MAPbI_3$ (3D)	20.65	1.078	79	17.6	negligible hysteresis with NO_x as HTL	[245]
$MAPbI_3$ (3D)	23.36	1.04	69.2	16.79	increased number of nucleation sites	[246]
$MAPbI_3$ (3D)	22.6	1.05	72	17.1	>1 cm^2 area performance	[247]
$CsPbI_2Br$ (3D)	15.33	1.22	78.7	14.78	slower perovskite film crystallization	[248]
$CsPbI_2Br$ (3D)	14.9	1.18	77.2	13.5	shorter reaction time needed	[249]
$Cs_{0.05}(FA_{0.83}MA_{0.17})_{0.95}Pb(I_{0.82}Br_{0.18})_3$ (3D)	19.02	1.791	74.6	25.2	record for highest efficiency in 3D perovskite	[250]
$(FAPbI_3)_x(MAPbI_3)_{1-x}$(3D)	23.7	1.12	76	20.2	uniform film and low recombination	[251]
$FAPbI_3$ (3D)	24.5	1.07	74.5	19.5	long carrier lifetime and diffusion	[252]
$Cs_{0.05}(Ma_{0.17}FA_{0.83})_{0.95}Pb(I_{0.83}Br_{0.17})_3$ (2D/3D)	23.15	1.05	–	17	less sensitivity to processing conditions	[253]
$Cs_{0.05}(Ma_{0.17}FA_{0.83})_{0.95}Pb(I_{0.83}Cl_{0.17})_3$ (2D/3D)	17.6	1.05	–	13.5	great stability for a few days in ambient conditions	[253]
$MAPbI_3$:g-C_3N_4 (2D)	24.31	1.07	74	19.49	DMF solvent	[254]
$FA_{0.85}MA_{0.15}Pb(I_{0.85}\ Br_{0.15})$ (2D)	21.8	1.15	74	18.73	additive used was nitrogen-doped reduced graphene oxide	[255]
$BDAPbI_4$ (1D)	20.5	0.97	71	14.1	forward Scan	[230]
$BDAPbI_4$ (1D)	20.5	0.96	70	13.8	reverse Scan	[230]
$CsPbI_3$ (0D)	13.47	1.23	65	10.77	quantum dots solution	[256]
$MASb_2I_9$ (0D)	1.4	0.74	–	0.54	best antimony based QD solution	[257]

4) Recently, 2D and 3D perovskites have been combined to increase stability, while maintaining an acceptable efficiency. Such synergistic combinations have not been researched as much when it comes to 1D and 0D materials. Their electrical capabilities may prove to be a crucial addition to either 2D or 3D/2D hybrids, in order to maximize the electrical output while maintaining a high stability over time.

5) Lastly, consistent production of higher quality thin films for all dimensions that maintain their electrical properties after scale-up is a major issue that has yet to be fully addressed in photodetectors and solar cells. There have been clear improvements in this area throughout the years, however, the technique is far from being streamlined, which will impact the adoption of these materials by the industry. Therefore, further research in high quality large-area growth methods is crucial going forward.

Acknowledgements The authors acknowledge the financial support from the Natural Sciences and Engineering Research Council of Canada through the Discovery Grant Program, the support of Canada Foundation for Innovation through John R. Evans Leaders Fund, the support through New Frontier in Research Fund, Dr. Robert Gillespie through the Dr Robert Gillespie graduate Scholarship, and the Pengrowth–Nova Scotia Energy through the Pengrowth Energy Innovation Grant. The authors acknowledge the support of Dean Grijm, Mark Leblanc and Greg Everett in completing this project.

Conflicts of interest The authors declare no conflict of interest.

References

1. Manser J S, Christians J A, Kamat P V. Intriguing optoelectronic properties of metal halide perovskites. Chemical Reviews, 2016, 116(21): 12956–13008
2. Zhou C, Lin H, He Q, Xu L, Worku M, Chaaban M, Lee S, Shi X, Du M H, Ma B. Low dimensional metal halide perovskites and hybrids. Materials Science and Engineering R Reports, 2019, 137: 38–65
3. Shi E, Gao Y, Finkenauer B P, Akriti, Coffey A H, Dou L. Two-dimensional halide perovskite nanomaterials and heterostructures. Chemical Society Reviews, 2018, 47(16): 6046–6072
4. Shi E, Dou L. A leap towards high-performance 2D perovskite photodetectors. Trends in Chemistry, 2019, 1(4): 365–367
5. Ma S, Cai M, Cheng T, Ding X, Shi X, Alsaedi A, Hayat T, Ding Y, Tan Z, Dai S. Two-dimensional organic-inorganic hybrid perovskite: from material properties to device applications. Science China Materials, 2018, 61(10): 1257–1277
6. Hong K, Van Le Q, Kim S Y, Jang H W. Low-dimensional halide perovskites: review and issues. Journal of Materials Chemistry C, Materials for Optical and Electronic Devices, 2018, 6(9): 2189–2209
7. Chao L, Wang Z, Xia Y, Chen Y, Huang W. Recent progress on low dimensional perovskite solar cells. Journal of Energy Chemistry, 2018, 27(4): 1091–1100
8. Park N G. Research direction toward scalable, stable, and high efficiency perovskite solar cells. Advanced Energy Materials, 2020, 10(13): 1903106
9. Zhang J, Yang X, Deng H, Qiao K, Farooq U, Ishaq M, Yi F, Liu H, Tang J, Song H. Low-dimensional halide perovskites and their advanced optoelectronic applications. Nano-Micro Letters, 2017, 9(3): 36
10. Forgacs D, Wojciechowski K, Malinkiewicz O. Perovskite Photovoltaics: From Laboratory to Industry. In: Petrova-Koch V, Hezel R, Goetzberger A, eds. High-Efficient Low-Cost Photovoltaics. Cham: Springer, 2020, 219–255
11. McMeekin D P, Wang Z, Rehman W, Pulvirenti F, Patel J B, Noel N K, Johnston M B, Marder S R, Herz L M, Snaith H J. Crystallization kinetics and morphology control of formamidinium-cesium mixed-cation lead mixed-halide perovskite via tunability of the colloidal precursor solution. Advanced Materials, 2017, 29(29): 1607039
12. Liu C, Cheng Y B, Ge Z. Understanding of perovskite crystal growth and film formation in scalable deposition processes. Chemical Society Reviews, 2020, 49(6): 1653–1687
13. Tyagi P, Arveson S M, Tisdale W A. Colloidal organohalide perovskite nanoplatelets exhibiting quantum confinement. Journal of Physical Chemistry Letters, 2015, 6(10): 1911–1916
14. Stranks S D, Eperon G E, Grancini G, Menelaou C, Alcocer M J, Leijtens T, Herz L M, Petrozza A, Snaith H J. Electron-hole diffusion lengths exceeding 1 micrometer in an organometal trihalide perovskite absorber. Science, 2013, 342(6156): 341–344
15. Stoumpos C C, Malliakas C D, Kanatzidis M G. Semiconducting tin and lead iodide perovskites with organic cations: phase transitions, high mobilities, and near-infrared photoluminescent properties. Inorganic Chemistry, 2013, 52(15): 9019–9038
16. Edri E, Kirmayer S, Kulbak M, Hodes G, Cahen D. Chloride inclusion and hole transport material doping to improve methyl ammonium lead bromide perovskite-based high open-circuit voltage solar cells. Journal of Physical Chemistry Letters, 2014, 5(3): 429–433
17. Noel N K, Stranks S D, Abate A, Wehrenfennig C, Guarnera S, Haghighirad A A, Sadhanala A, Eperon G E, Pathak S K, Johnston M B, Petrozza A, Herz L M, Snaith H J. Lead-free organic–inorganic tin halide perovskites for photovoltaic applications. Energy & Environmental Science, 2014, 7(9): 3061–3068
18. Tan K W, Moore D T, Saliba M, Sai H, Estroff L A, Hanrath T, Snaith H J, Wiesner U. Thermally induced structural evolution and performance of mesoporous block copolymer-directed alumina perovskite solar cells. ACS Nano, 2014, 8(5): 4730–4739
19. D'Innocenzo V, Grancini G, Alcocer M J, Kandada A R S, Stranks S D, Lee M M, Lanzani G, Snaith H J, Petrozza A. Excitons versus free charges in organo-lead tri-halide perovskites. Nature Communications, 2014, 5(1): 3586
20. Qian L, Sun Y, Wu M, Li C, Xie D, Ding L, Shi G. A lead-free two-dimensional perovskite for a high-performance flexible photoconductor and a light-stimulated synaptic device. Nanoscale, 2018, 10(15): 6837–6843
21. Hossain A, Roy S, Sakthipandi K. The external and internal influences on the tuning of the properties of perovskites: an overview. Ceramics International, 2019, 45(4): 4152–4166
22. Kitazawa N, Watanabe Y, Nakamura Y. Optical properties of $CH_3NH_3PbX_3$ (X = halogen) and their mixed-halide crystals.

Journal of Materials Science, 2002, 37(17): 3585–3587
23. Noh J H, Im S H, Heo J H, Mandal T N, Seok S I. Chemical management for colorful, efficient, and stable inorganic–organic hybrid nanostructured solar cells. Nano Letters, 2013, 13(4): 1764–1769
24. Protesescu L, Yakunin S, Bodnarchuk M I, Krieg F, Caputo R, Hendon C H, Yang R X, Walsh A, Kovalenko M V. Nanocrystals of cesium lead halide perovskites ($CsPbX_3$, X = Cl, Br, and I): novel optoelectronic materials showing bright emission with wide color gamut. Nano Letters, 2015, 15(6): 3692–3696
25. Dubey A, Adhikari N, Mabrouk S, Wu F, Chen K, Yang S, Qiao Q. A strategic review on processing routes towards highly efficient perovskite solar cells. Journal of Materials Chemistry A, Materials for Energy and Sustainability, 2018, 6(6): 2406–2431
26. Wang P, Zhang X, Zhou Y, Jiang Q, Ye Q, Chu Z, Li X, Yang X, Yin Z, You J. Solvent-controlled growth of inorganic perovskite films in dry environment for efficient and stable solar cells. Nature Communications, 2018, 9(1): 2225
27. Chilvery A, Das S, Guggilla P, Brantley C, Sunda-Meya A. A perspective on the recent progress in solution-processed methods for highly efficient perovskite solar cells. Science and Technology of Advanced Materials, 2016, 17(1): 650–658
28. Kong W, Wang G, Zheng J, Hu H, Chen H, Li Y, Hu M, Zhou X, Liu C, Chandrashekar B N, Amini A, Wang J, Xu B, Cheng C. Fabricating high-efficient blade-coated perovskite solar cells under ambient condition using lead acetate trihydrate. Solar RRL, 2018, 2(3): 1700214
29. Li C, Yin J, Chen R, Lv X, Feng X, Wu Y, Cao J. Monoammonium porphyrin for blade-coating stable large-area perovskite solar cells with > 18% efficiency. Journal of the American Chemical Society, 2019, 141(15): 6345–6351
30. Sun S, Yuan D, Xu Y, Wang A, Deng Z. Ligand-mediated synthesis of shape-controlled cesium lead halide perovskite nanocrystals via reprecipitation process at room temperature. ACS Nano, 2016, 10(3): 3648–3657
31. Lan C, Zhou Z, Wei R, Ho J C. Two-dimensional perovskite materials: from synthesis to energy-related applications. Materials Today Energy, 2019, 11: 61–82
32. Even J, Pedesseau L, Katan C. Understanding quantum confinement of charge carriers in layered 2D hybrid perovskites. ChemPhysChem, 2014, 15(17): 3733–3741
33. Green M, Ho-Baillie A, Snaith H. The emergence of perovskite solar cells. Nature Photonics, 2014, 8: 506–514
34. Ahmadi M, Wu T, Hu B. A review on organic–inorganic halide perovskite photodetectors: device engineering and fundamental physics. Advanced Materials, 2017, 29(41): 1605242
35. Nayak P K, Moore D T, Wenger B, Nayak S, Haghighirad A A, Fineberg A, Noel N K, Reid O G, Rumbles G, Kukura P, Vincent K A, Snaith H J. Mechanism for rapid growth of organic-inorganic halide perovskite crystals. Nature Communications, 2016, 7(1): 13303
36. Wu K, Bera A, Ma C, Du Y, Yang Y, Li L, Wu T. Temperature-dependent excitonic photoluminescence of hybrid organometal halide perovskite films. Physical Chemistry Chemical Physics, 2014, 16(41): 22476–22481
37. Papavassiliou G C, Koutselas I B. Structural, optical and related properties of some natural three-and lower-dimensional semiconductor systems. Synthetic Metals, 1995, 71(1–3): 1713–1714
38. Mehrabian M, Dalir S, Mahmoudi G, Miroslaw B, Babashkina M G, Dektereva A V, Safin D A. A highly stable all-inorganic $CsPbBr_3$ perovskite solar cell. European Journal of Inorganic Chemistry, 2019, 2019(32): 3699–3703
39. Ling Y, Yuan Z, Tian Y, Wang X, Wang J C, Xin Y, Hanson K, Ma B, Gao H. Bright light-emitting diodes based on organometal halide perovskite nanoplatelets. Advanced Materials, 2016, 28(2): 305–311
40. Kojima A, Teshima K, Shirai Y, Miyasaka T. Organometal halide perovskites as visible-light sensitizers for photovoltaic cells. Journal of the American Chemical Society, 2009, 131(17): 6050–6051
41. Hu Y, Spies L M, Alonso-Álvarez D, Mocherla P, Jones H, Hanisch J, Bein T, Barnes P R F, Docampo P. Identifying and controlling phase purity in 2D hybrid perovskite thin films. Journal of Materials Chemistry A, Materials for Energy and Sustainability, 2018, 6(44): 22215–22225
42. Zhang X, Ren X, Liu B, Munir R, Zhu X, Yang D, Li J, Liu Y, Smilgies D M, Li R, Yang Z, Niu T, Wang X, Amassian A, Zhao K, Liu S F. Stable high efficiency two-dimensional perovskite solar cells via cesium doping. Energy & Environmental Science, 2017, 10(10): 2095–2102
43. Bekenstein Y, Koscher B A, Eaton S W, Yang P, Alivisatos A P. Highly luminescent colloidal nanoplates of perovskite cesium lead halide and their oriented assemblies. Journal of the American Chemical Society, 2015, 137(51): 16008–16011
44. Shamsi J, Dang Z, Bianchini P, Canale C, Stasio F D, Brescia R, Prato M, Manna L. Colloidal synthesis of quantum confined single crystal $CsPbBr_3$ nanosheets with lateral size control up to the micrometer range. Journal of the American Chemical Society, 2016, 138(23): 7240–7243
45. Yuan Z, Shu Y, Tian Y, Xin Y, Ma B. A facile one-pot synthesis of deep blue luminescent lead bromide perovskite microdisks. Chemical Communications, 2015, 51(91): 16385–16388
46. Sichert J A, Tong Y, Mutz N, Vollmer M, Fischer S, Milowska K Z, García Cortadella R, Nickel B, Cardenas-Daw C, Stolarczyk J K, Urban A S, Feldmann J. Quantum size effect in organometal halide perovskite nanoplatelets. Nano Letters, 2015, 15(10): 6521–6527
47. Dou L, Wong A B, Yu Y, Lai M, Kornienko N, Eaton S W, Fu A, Bischak C G, Ma J, Ding T, Ginsberg N S, Wang L W, Alivisatos A P, Yang P. Atomically thin two-dimensional organic-inorganic hybrid perovskites. Science, 2015, 349(6255): 1518–1521
48. Hintermayr V A, Richter A F, Ehrat F, Döblinger M, Vanderlinden W, Sichert J A, Tong Y, Polavarapu L, Feldmann J, Urban A S. Tuning the optical properties of perovskite nanoplatelets through composition and thickness by ligand-assisted exfoliation. Advanced Materials, 2016, 28(43): 9478–9485
49. Ha S T, Liu X, Zhang Q, Giovanni D, Sum T C, Xiong Q. Synthesis of organic–inorganic lead halide perovskite nanoplatelets: towards high-performance perovskite solar cells and optoelectronic devices. Advanced Optical Materials, 2014, 2(9): 838–844
50. Schmidt L C, Pertegás A, González-Carrero S, Malinkiewicz O,

Agouram S, Mínguez Espallargas G, Bolink H J, Galian R E, Pérez-Prieto J. Nontemplate synthesis of $CH_3NH_3PbBr_3$ perovskite nanoparticles. Journal of the American Chemical Society, 2014, 136(3): 850–853

51. Ma C, Shen D, Ng T W, Lo M F, Lee C S. 2D perovskites with short interlayer distance for high-performance solar cell application. Advanced Materials, 2018, 30(22): 1800710
52. Liang D, Peng Y, Fu Y, Shearer M J, Zhang J, Zhai J, Zhang Y, Hamers R J, Andrew T L, Jin S. Color-pure violet-light-emitting diodes based on layered lead halide perovskite nanoplates. ACS Nano, 2016, 10(7): 6897–6904
53. Liu Y, Ye H, Zhang Y, Zhao K, Yang Z, Yuan Y, Wu H, Zhao G, Yang Z, Tang J, Xu Z, Liu S F. Surface-tension-controlled crystallization for high-quality 2D perovskite single crystals for ultrahigh photodetection. Matter, 2019, 1(2): 465–480
54. Niu T, Ren H, Wu B, Xia Y, Xie X, Yang Y, Gao X, Chen Y, Huang W. Reduced-dimensional perovskite enabled by organic diamine for efficient photovoltaics. Journal of Physical Chemistry Letters, 2019, 10(10): 2349–2356
55. Zhang X, Munir R, Xu Z, Liu Y, Tsai H, Nie W, Li J, Niu T, Smilgies D M, Kanatzidis M G, Mohite A D, Zhao K, Amassian A, Liu S F. Phase transition control for high performance Ruddlesden–Popper perovskite solar cells. Advanced Materials, 2018, 30(21): 1707166
56. Ke W, Mao L, Stoumpos C C, Hoffman J, Spanopoulos I, Mohite A D, Kanatzidis M G. Compositional and solvent engineering in Dion–Jacobson 2D perovskites boosts solar cell efficiency and stability. Advanced Energy Materials, 2019, 9(10): 1803384
57. Hasan M M, Clegg C, Manning M, El Ghanam A, Su C, Harding M D, Bennett C, Hill I G, Koleilat G I. Stable efficient methylammonium lead iodide thin film photodetectors with highly oriented millimeter-sized crystal grains. ACS Photonics, 2020, 7 (1): 57–67
58. Wang K, Wu C, Yang D, Jiang Y, Priya S. Quasi-two-dimensional halide perovskite single crystal photodetector. ACS Nano, 2018, 12(5): 4919–4929
59. Quan L N, Yuan M, Comin R, Voznyy O, Beauregard E M, Hoogland S, Buin A, Kirmani A R, Zhao K, Amassian A, Kim D H, Sargent E H. Ligand-stabilized reduced-dimensionality perovskites. Journal of the American Chemical Society, 2016, 138(8): 2649–2655
60. Tsai H, Nie W, Blancon J C, Stoumpos C C, Asadpour R, Harutyunyan B, Neukirch A J, Verduzco R, Crochet J J, Tretiak S, Pedesseau L, Even J, Alam M A, Gupta G, Lou J, Ajayan P M, Bedzyk M J, Kanatzidis M G, Mohite A D. High-efficiency two-dimensional Ruddlesden-Popper perovskite solar cells. Nature, 2016, 536(7616): 312–316
61. Ono L K, Qi Y. Research progress on organic–inorganic halide perovskite materials and solar cells. Journal of Physics. D, Applied Physics, 2018, 51(9): 093001
62. Ren H, Yu S, Chao L, Xia Y, Sun Y, Zuo S, Li F, Niu T, Yang Y, Ju H, Li B, Du H, Gao X, Zhang J, Wang J, Zhang L, Chen Y, Huang W. Efficient and stable Ruddlesden–Popper perovskite solar cell with tailored interlayer molecular interaction. Nature Photonics, 2020, 14(3): 154–163
63. Stoumpos C C, Cao D H, Clark D J, Young J, Rondinelli J M, Jang J I, Hupp J T, Kanatzidis M G. Ruddlesden–Popper hybrid lead iodide perovskite 2D homologous semiconductors. Chemistry of Materials, 2016, 28(8): 2852–2867
64. Wu G, Li X, Zhou J, Zhang J, Zhang X, Leng X, Wang P, Chen M, Zhang D, Zhao K, Liu S F, Zhou H, Zhang Y. Fine multi-phase alignments in 2D perovskite solar cells with efficiency over 17% via slow post-annealing. Advanced Materials, 2019, 31(42): 1903889
65. Ma L, Ju M G, Dai J, Zeng X C. Tin and germanium based two-dimensional Ruddlesden–Popper hybrid perovskites for potential lead-free photovoltaic and photoelectronic applications. Nanoscale, 2018, 10(24): 11314–11319
66. Cheng P, Wu T, Liu J, Deng W Q, Han K. Lead-free, two-dimensional mixed germanium and tin perovskites. Journal of Physical Chemistry Letters, 2018, 9(10): 2518–2522
67. Byun J, Cho H, Wolf C, Jang M, Sadhanala A, Friend R H, Yang H, Lee T W. Efficient visible quasi-2D perovskite light-emitting diodes. Advanced Materials, 2016, 28(34): 7515–7520
68. Soe C M M, Stoumpos C C, Kepenekian M, Traoré B, Tsai H, Nie W, Wang B, Katan C, Seshadri R, Mohite A D, Even J, Marks T J, Kanatzidis M G. New type of 2D perovskites with alternating cations in the interlayer space, $(C(NH_2)_3)(CH_3NH_3)_nPb_nI_{3n+1}$: structure, properties, and photovoltaic performance. Journal of the American Chemical Society, 2017, 139(45): 16297–16309
69. Wang N, Cheng L, Ge R, Zhang S, Miao Y, Zou W, Yi C, Sun Y, Cao Y, Yang R, Wei Y, Guo Q, Ke Y, Yu M, Jin Y, Liu Y, Ding Q, Di D, Yang L, Xing G, Tian H, Jin C, Gao F, Friend R H, Wang J, Huang W. Perovskite light-emitting diodes based on solution-processed self-organized multiple quantum wells. Nature Photonics, 2016, 10(11): 699–704
70. Zheng H, Liu G, Zhu L, Ye J, Zhang X, Alsaedi A, Hayat T, Pan X, Dai S. The effect of hydrophobicity of ammonium salts on stability of quasi-2D perovskite materials in moist condition. Advanced Energy Materials, 2018, 8(21): 1800051
71. Yao K, Wang X, Xu Y X, Li F, Zhou L. Multilayered perovskite materials based on polymeric-ammonium cations for stable large-area solar cell. Chemistry of Materials, 2016, 28(9): 3131–3138
72. Lai H, Kan B, Liu T, Zheng N, Xie Z, Zhou T, Wan X, Zhang X, Liu Y, Chen Y. Two-dimensional Ruddlesden–Popper perovskite with nanorod-like morphology for solar cells with efficiency exceeding 15%. Journal of the American Chemical Society, 2018, 140(37): 11639–11646
73. Proppe A H, Quintero-Bermudez R, Tan H, Voznyy O, Kelley S O, Sargent E H. Synthetic control over quantum well width distribution and carrier migration in low-dimensional perovskite photovoltaics. Journal of the American Chemical Society, 2018, 140(8): 2890–2896
74. Stoumpos C C, Soe C M M, Tsai H, Nie W, Blancon J C, Cao D H, Liu F, Traoré B, Katan C, Even J, Mohite A D, Kanatzidis M G. High members of the 2D Ruddlesden-Popper halide perovskites: synthesis, optical properties, and solar cells of $(CH_3(CH_2)_3NH_3)_2(CH_3NH_3)_4Pb_5I_{16}$. Chem, 2017, 2(3): 427–440
75. Fraccarollo A, Canti L, Marchese L, Cossi M. First principles study of 2D layered organohalide tin perovskites. Journal of Chemical Physics, 2017, 146(23): 234703
76. Koutselas I B, Ducasse L, Papavassiliou G C. Electronic properties

of three-and low-dimensional semiconducting materials with Pb halide and Sn halide units. Journal of Physics Condensed Matter, 1996, 8(9): 1217–1227

77. Liu J, Leng J, Wu K, Zhang J, Jin S. Observation of internal photoinduced electron and hole separation in hybrid two-dimentional perovskite films. Journal of the American Chemical Society, 2017, 139(4): 1432–1435
78. Yuan M, Quan L N, Comin R, Walters G, Sabatini R, Voznyy O, Hoogland S, Zhao Y, Beauregard E M, Kanjanaboos P, Lu Z, Kim D H, Sargent E H. Perovskite energy funnels for efficient light-emitting diodes. Nature Nanotechnology, 2016, 11(10): 872–877
79. Kwon H C, Yang W, Lee D, Ahn J, Lee E, Ma S, Kim K, Yun S C, Moon J. Investigating recombination and charge carrier dynamics in a one-dimensional nanopillared perovskite absorber. ACS Nano, 2018, 12(5): 4233–4245
80. Du W, Zhang S, Shi J, Chen J, Wu Z, Mi Y, Liu Z, Li Y, Sui X, Wang R, Qiu X, Wu T, Xiao Y, Zhang Q, Liu X. Strong exciton–photon coupling and lasing behavior in all-inorganic $CsPbBr_3$ micro/nanowire Fabry-Pérot cavity. ACS Photonics, 2018, 5(5): 2051–2059
81. Xu X, Zhang X, Deng W, Jie J, Zhang X. 1D organic–inorganic hybrid perovskite micro/nanocrystals: fabrication, assembly, and optoelectronic applications. Small Methods, 2018, 2(7): 1700340
82. Ha S T, Su R, Xing J, Zhang Q, Xiong Q. Metal halide perovskite nanomaterials: synthesis and applications. Chemical Science (Cambridge), 2017, 8(4): 2522–2536
83. Horváth E, Spina M, Szekrényes Z, Kamarás K, Gaal R, Gachet D, Forró L. Nanowires of methylammonium lead iodide ($CH_3NH_3PbI_3$) prepared by low temperature solution-mediated crystallization. Nano Letters, 2014, 14(12): 6761–6766
84. Zhang D, Eaton S W, Yu Y, Dou L, Yang P. Solution-phase synthesis of cesium lead halide perovskite nanowires. Journal of the American Chemical Society, 2015, 137(29): 9230–9233
85. Xing J, Liu X F, Zhang Q, Ha S T, Yuan Y W, Shen C, Sum T C, Xiong Q. Vapor phase synthesis of organometal halide perovskite nanowires for tunable room-temperature nanolasers. Nano Letters, 2015, 15(7): 4571–4577
86. Chen L J, Lee C R, Chuang Y J, Wu Z H, Chen C. Synthesis and optical properties of lead-free cesium tin halide perovskite quantum rods with high-performance solar cell application. Journal of Physical Chemistry Letters, 2016, 7(24): 5028–5035
87. Wong A B, Lai M, Eaton S W, Yu Y, Lin E, Dou L, Fu A, Yang P. Growth and anion exchange conversion of $CH_3NH_3PbX_3$ nanorod arrays for light-emitting diodes. Nano Letters, 2015, 15(8): 5519–5524
88. Chen P, Bai Y, Lyu M, Yun J H, Hao M, Wang L. Progress and perspective in low-dimensional metal halide perovskites for optoelectronic applications. Solar RRL, 2018, 2(3): 1700186
89. Yuan Z, Zhou C, Tian Y, Shu Y, Messier J, Wang J C, van de Burgt L J, Kountouriotis K, Xin Y, Holt E, Schanze K, Clark R, Siegrist T, Ma B. One-dimensional organic lead halide perovskites with efficient bluish white-light emission. Nature Communications, 2017, 8(1): 14051
90. Jung M H. Broadband white light emission from one-dimensional zigzag edge-sharing perovskite. New Journal of Chemistry, 2020, 44(1): 171–180
91. Li X, Wu Y, Zhang S, Cai B, Gu Y, Song J, Zeng H. $CsPbX_3$ quantum dots for lighting and displays: room-temperature synthesis, photoluminescence superiorities, underlying origins and white light-emitting diodes. Advanced Functional Materials, 2016, 26(15): 2435–2445
92. Zhou Q, Bai Z, Lu W G, Wang Y, Zou B, Zhong H. *In situ* fabrication of halide perovskite nanocrystal-embedded polymer composite films with enhanced photoluminescence for display backlights. Advanced Materials, 2016, 28(41): 9163–9168
93. Zhao L, Yeh Y W, Tran N L, Wu F, Xiao Z, Kerner R A, Lin Y L, Scholes G D, Yao N, Rand B P. *In situ* preparation of metal halide perovskite nanocrystal thin films for improved light-emitting devices. ACS Nano, 2017, 11(4): 3957–3964
94. Liu J, Hu F, Zhou Y, Zhang C, Wang X, Xiao M. Polarized emission from single perovskite $FAPbBr_3$ nanocrystals. Journal of Luminescence, 2020, 221: 117032
95. Nikl M, Mihokova E, Nitsch K, Somma F, Giampaolo C, Pazzi G P, Fabeni P, Zazubovich S. Photoluminescence of Cs_4PbBr_6 crystals and thin films. Chemical Physics Letters, 1999, 306(5–6): 280–284
96. Han D, Shi H, Ming W, Zhou C, Ma B, Saparov B, Ma Y Z, Chen S, Du M H. Unraveling luminescence mechanisms in zero-dimensional halide perovskites. Journal of Materials Chemistry C, Materials for Optical and Electronic Devices, 2018, 6(24): 6398–6405
97. Xu L J, Sun C Z, Xiao H, Wu Y, Chen Z N. Green-light-emitting diodes based on tetrabromide manganese (II) complex through solution process. Advanced Materials, 2017, 29(10): 1605739
98. Worku M, Xu L J, Chaaban M, Ben-Akacha A, Ma B. Optically pumped white light-emitting diodes based on metal halide perovskites and perovskite-related materials. APL Materials, 2020, 8(1): 010902
99. Hebig J C, Kühn I, Flohre J, Kirchartz T. Optoelectronic properties of $(CH_3NH_3)_3Sb_2I_9$ thin films for photovoltaic applications. ACS Energy Letters, 2016, 1(1): 309–314
100. Öz S, Hebig J C, Jung E, Singh T, Lepcha A, Olthof S, Jan F, Gao Y, German R, van Loosdrecht P H M, Meerholz K, Kirchartz T, Mathur S. Zero-dimensional $(CH_3NH_3)_3Bi_2I_9$ perovskite for optoelectronic applications. Solar Energy Materials and Solar Cells, 2016, 158: 195–201
101. Pious J K, Lekshmi M L, Muthu C, Rakhi R B, Nair V C. Zero-dimensional methylammonium bismuth iodide-based lead-free perovskite capacitor. ACS Omega, 2017, 2(9): 5798–5802
102. Sun S, Salim T, Mathews N, Duchamp M, Boothroyd C, Xing G, Sum T C, Lam Y M. The origin of high efficiency in low-temperature solution-processable bilayer organometal halide hybrid solar cells. Energy & Environmental Science, 2014, 7(1): 399–407
103. Ponseca C S Jr, Savenije T J, Abdellah M, Zheng K, Yartsev A, Pascher T, Harlang T, Chabera P, Pullerits T, Stepanov A, Wolf J P, Sundström V. Organometal halide perovskite solar cell materials rationalized: ultrafast charge generation, high and microsecond-long balanced mobilities, and slow recombination. Journal of the American Chemical Society, 2014, 136(14): 5189–5192
104. Dong C R, Wang Y, Zhang K, Zeng H. Halide perovskite materials as light harvesters for solar energy conversion. EnergyChem, 2020,

2(1): 100026

105. Sweeney S J, Mukherjee J. Optoelectronic Devices and Materials. In: Kasap S, Capper P, eds. Springer Handbook of Electronic and Photonic Materials. Cham: Springer, 2017
106. Eperon G E, Leijtens T, Bush K A, Prasanna R, Green T, Wang J T, McMeekin D P, Volonakis G, Milot R L, May R, Palmstrom A, Slotcavage D J, Belisle R A, Patel J B, Parrott E S, Sutton R J, Ma W, Moghadam F, Conings B, Babayigit A, Boyen H G, Bent S, Giustino F, Herz L M, Johnston M B, McGehee M D, Snaith H J. Perovskite-perovskite tandem photovoltaics with optimized band gaps. Science, 2016, 354(6314): 861–865
107. Sarritzu V, Sestu N, Marongiu D, Chang X, Wang Q, Masi S, Colella S, Rizzo A, Gocalinska A, Pelucchi E, Mercuri M L, Quochi F, Saba M, Mura A, Bongiovanni G. Direct or indirect bandgap in hybrid lead halide perovskites? Advanced Optical Materials, 2018, 6(10): 1701254
108. Hutter E M, Gélvez-Rueda M C, Osherov A, Bulović V, Grozema F C, Stranks S D, Savenije T J. Direct-indirect character of the bandgap in methylammonium lead iodide perovskite. Nature Materials, 2017, 16(1): 115–120
109. Brenes R, Guo D, Osherov A, Noel N K, Eames C, Hutter E M, Pathak S K, Niroui F, Friend R H, Islam M S, Snaith H J, Bulović V, Savenije T J, Stranks S D. Metal halide perovskite polycrystalline films exhibiting properties of single crystals. Joule, 2017, 1(1): 155–167
110. Saba M, Cadelano M, Marongiu D, Chen F, Sarritzu V, Sestu N, Figus C, Aresti M, Piras R, Lehmann A G, Cannas C, Musinu A, Quochi F, Mura A, Bongiovanni G. Correlated electron-hole plasma in organometal perovskites. Nature Communications, 2014, 5(1): 5049
111. Tao S X, Cao X, Bobbert P A. Accurate and efficient band gap predictions of metal halide perovskites using the DFT-1/2 method: GW accuracy with DFT expense. Scientific Reports, 2017, 7(1): 14386
112. Srimath Kandada A R, Neutzner S, D'Innocenzo V, Tassone F, Gandini M, Akkerman Q A, Prato M, Manna L, Petrozza A, Lanzani G. Nonlinear carrier interactions in lead halide perovskites and the role of defects. Journal of the American Chemical Society, 2016, 138(41): 13604–13611
113. Ke W, Kanatzidis M G. Prospects for low-toxicity lead-free perovskite solar cells. Nature Communications, 2019, 10(1): 965
114. Gao P, Grätzel M, Nazeeruddin M K. Organohalide lead perovskites for photovoltaic applications. Energy & Environmental Science, 2014, 7(8): 2448–2463
115. Kulkarni S A, Baikie T, Boix P P, Yantara N, Mathews N, Mhaisalkar S. Band-gap tuning of lead halide perovskites using a sequential deposition process. Journal of Materials Chemistry A, Materials for Energy and Sustainability, 2014, 2(24): 9221–9225
116. Eperon G E, Stranks S D, Menelaou C, Johnston M B, Herz L M, Snaith H J. Formamidinium lead trihalide: a broadly tunable perovskite for efficient planar heterojunction solar cells. Energy & Environmental Science, 2014, 7(3): 982
117. Levchuk I, Osvet A, Tang X, Brandl M, Perea J D, Hoegl F, Matt G J, Hock R, Batentschuk M, Brabec C J. Brightly luminescent and color-tunable formamidinium lead halide perovskite $FAPbX_3$ (X = Cl, Br, I) colloidal nanocrystals. Nano Letters, 2017, 17(5): 2765–2770
118. Wang S, Sakurai T, Wen W, Qi Y. Energy level alignment at interfaces in metal halide perovskite solar cells. Advanced Materials Interfaces, 2018, 5(22): 1800260
119. Kieslich G, Sun S, Cheetham A K. An extended tolerance factor approach for organic–inorganic perovskites. Chemical Science (Cambridge), 2015, 6(6): 3430–3433
120. Filip M R, Eperon G E, Snaith H J, Giustino F. Steric engineering of metal-halide perovskites with tunable optical band gaps. Nature Communications, 2014, 5(1): 5757
121. Ou Q, Bao X, Zhang Y, Shao H, Xing G, Li X, Shao L, Bao Q. Band structure engineering in metal halide perovskite nanostructures for optoelectronic applications. Nano Materials Science, 2019, 1(4): 268–287
122. Smith M D, Pedesseau L, Kepenekian M, Smith I C, Katan C, Even J, Karunadasa H I. Decreasing the electronic confinement in layered perovskites through intercalation. Chemical Science (Cambridge), 2017, 8(3): 1960–1968
123. Fox M. Optical Properties of Solids. Oxford: Oxford University Press, 2001
124. Mitzi D B. Synthesis, crystal structure, and optical and thermal properties of $(C_4H_9NH_3)_2MI_4$ (M = Ge, Sn, Pb). Chemistry of Materials, 1996, 8(3): 791–800
125. Pandey M, Jacobsen K W, Thygesen K S. Band gap tuning and defect tolerance of atomically thin two-dimensional organic-inorganic halide perovskites. Journal of Physical Chemistry Letters, 2016, 7(21): 4346–4352
126. Lanty G, Jemli K, Wei Y, Leymarie J, Even J, Lauret J S, Deleporte E. Room-temperature optical tunability and inhomogeneous broadening in 2D-layered organic-inorganic perovskite pseudo-binary alloys. Journal of Physical Chemistry Letters, 2014, 5(22): 3958–3963
127. Weidman M C, Seitz M, Stranks S D, Tisdale W A. Highly tunable colloidal perovskite nanoplatelets through variable cation, metal, and halide composition. ACS Nano, 2016, 10(8): 7830–7839
128. Tanaka K, Kondo T. Bandgap and exciton binding energies in lead-iodide based natural quantum-well crystals. Science and Technology of Advanced Materials, 2003, 4(6): 599–604
129. Vashishtha P, Metin D Z, Cryer M E, Chen K, Hodgkiss J M, Gaston N, Halpert J E. Shape-, size-, and composition-controlled thallium lead halide perovskite nanowires and nanocrystals with tunable band gaps. Chemistry of Materials, 2018, 30(9): 2973–2982
130. Qiu T, Hu Y, Xu F, Yan Z, Bai F, Jia G, Zhang S. Recent advances in one-dimensional halide perovskites for optoelectronic applications. Nanoscale, 2018, 10(45): 20963–20989
131. Im J H, Lee C R, Lee J W, Park S W, Park N G. 6.5% efficient perovskite quantum-dot-sensitized solar cell. Nanoscale, 2011, 3 (10): 4088–4093
132. Li G, Liu Z, Huang Q, Gao Y, Regula M, Wang D, Chen L Q, Wang D. Stable metal battery anodes enabled by polyethylenimine sponge hosts by way of electrokinetic effects. Nature Energy, 2018, 3(12): 1076–1083
133. Zhang J, Bai D, Jin Z, Bian H, Wang K, Sun J, Wang Q, Liu S F. 3D–2D–0D interface profiling for record efficiency all-inorganic $CsPbBrI_2$ perovskite solar cells with superior stability. Advanced

Energy Materials, 2018, 8(15): 1703246
134. Wehrenfennig C, Eperon G E, Johnston M B, Snaith H J, Herz L M. High charge carrier mobilities and lifetimes in organolead trihalide perovskites. Advanced Materials, 2014, 26(10): 1584–1589
135. Verma J, Islam S M, Verma A, Protasenko V, Jena D. Nitride LEDs Based on Quantum Wells and Quantum Dots. In: Huang J J, Kuo H C, Shen S C, eds. Nitride Semiconductor Light-Emitting Diodes (LEDs): Materials, Technologies, and Applications, 2nd edition. Cambridge: Woodhead Publishing, 2018, 377–413
136. Meggiolaro D, Motti S G, Mosconi E, Barker A J, Ball J, Andrea Riccardo Perini C, Deschler F, Petrozza A, De Angelis F. Iodine chemistry determines the defect tolerance of lead-halide perovskites. Energy & Environmental Science, 2018, 11(3): 702–713
137. Herz L M. Charge-carrier dynamics in organic-inorganic metal halide perovskites. Annual Review of Physical Chemistry, 2016, 67(1): 65–89
138. Xing G, Wu B, Wu X, Li M, Du B, Wei Q, Guo J, Yeow E K, Sum T C, Huang W. Transcending the slow bimolecular recombination in lead-halide perovskites for electroluminescence. Nature Communications, 2017, 8(1): 14558
139. Xing G, Mathews N, Sun S, Lim S S, Lam Y M, Gratzel M, Mhaisalkar S, Sum T C. Long-range balanced electron- and hole-transport lengths in organic-inorganic $CH_3NH_3PbI_3$. Science, 2013, 342(6156): 344–347
140. Nie W, Tsai H, Asadpour R, Blancon J C, Neukirch A J, Gupta G, Crochet J J, Chhowalla M, Tretiak S, Alam M A, Wang H L, Mohite A D. High-efficiency solution-processed perovskite solar cells with millimeter-scale grains. Science, 2015, 347(6221): 522–525
141. Wu X, Trinh M T, Niesner D, Zhu H, Norman Z, Owen J S, Yaffe O, Kudisch B J, Zhu X Y. Trap states in lead iodide perovskites. Journal of the American Chemical Society, 2015, 137(5): 2089–2096
142. Zheng K, Zidek K, Abdellah M, Chen J, Chábera P, Zhang W, Al-Marri M J, Pullerits T. High excitation intensity opens a new trapping channel in organic–inorganic hybrid perovskite nanoparticles. ACS Energy Letters, 2016, 1(6): 1154–1161
143. Freppon D J, Men L, Burkhow S J, Petrich J W, Vela J, Smith E A. Photophysical properties of wavelength-tunable methylammonium lead halide perovskite nanocrystals. Journal of Materials Chemistry C, Materials for Optical and Electronic Devices, 2017, 5(1): 118–126
144. Jin H, Debroye E, Keshavarz M, Scheblykin I G, Roeffaers M B J, Hofkens J, Steele J A. It's a trap! On the nature of localised states and charge trapping in lead halide perovskites. Materials Horizons, 2020, 7(2): 397–410
145. Yang L, Dall'Agnese C, Dall'Agnese Y, Chen G, Gao Y, Sanehira Y, Jena A K, Wang X F, Gogotsi Y, Miyasaka T. Surface-modified metallic $Ti_3C_2T_x$ MXene as electron transport layer for planar heterojunction perovskite solar cells. Advanced Functional Materials, 2019, 29(46): 1905694
146. Lin Q, Armin A, Nagiri R C R, Burn P L, Meredith P. Electro-optics of perovskite solar cells. Nature Photonics, 2015, 9(2): 106–112
147. Even J, Pedesseau L, Katan C. Analysis of multivalley and multibandgap absorption and enhancement of free carriers related to exciton screening in hybrid perovskites. Journal of Physical Chemistry C, 2014, 118(22): 11566–11572
148. Galkowski K, Mitioglu A, Miyata A, Plochocka P, Portugall O, Eperon G E, Wang J T W, Stergiopoulos T, Stranks S D, Snaith H J, Nicholas R J. Determination of the exciton binding energy and effective masses for methylammonium and formamidinium lead tri-halide perovskite semiconductors. Energy & Environmental Science, 2016, 9(3): 962–970
149. Mauck C M, Tisdale W A. Excitons in 2D organic–inorganic halide perovskites. Trends in Chemistry, 2019, 4(1): 380–393
150. Munson K T, Kennehan E R, Doucette G S, Asbury J B. Dynamic disorder dominates delocalization, transport, and recombination in halide perovskites. Chem, 2018, 4(12): 2826–2843
151. Kim Y H, Kim J S, Lee T W. Strategies to improve luminescence efficiency of metal-halide perovskites and light-emitting diodes. Advanced Materials, 2019, 31(47): 1804595
152. Kim Y H, Wolf C, Kim H, Lee T W. Charge carrier recombination and ion migration in metal-halide perovskite nanoparticle films for efficient light-emitting diodes. Nano Energy, 2018, 52: 329–335
153. Shi E, Deng S, Yuan B, Gao Y, Akriti, Yuan L, Davis C S, Zemlyanov D, Yu Y, Huang L, Dou L. Extrinsic and dynamic edge states of two-dimensional lead halide perovskites. ACS Nano, 2019, 13(2): 1635–1644
154. Cheng B, Li T Y, Wei P C, Yin J, Ho K T, Retamal J R D, Mohammed O F, He J H. Layer-edge device of two-dimensional hybrid perovskites. Nature Communications, 2018, 9(1): 5196
155. Thomson S. Measuring Charge Carrier Lifetime in Halide Perovskite Using Time-Resolved Photoluminescence Spectroscopy. Edinburgh Instruments, 2018, 23
156. Han Q, Bae S H, Sun P, Hsieh Y T, Yang Y M, Rim Y S, Zhao H, Chen Q, Shi W, Li G, Yang Y. Single crystal formamidinium lead iodide ($FAPbI_3$): insight into the structural, optical, and electrical properties. Advanced Materials, 2016, 28(11): 2253–2258
157. Yang B, Han K. Charge-carrier dynamics of lead-free halide perovskite nanocrystals. Accounts of Chemical Research, 2019, 52(11): 3188–3198
158. Zhi R, Hu J, Yang S, Perumal Veeramalai C, Zhang Z, Saleem M I, Sulaman M, Tang Y, Zou B. A facile method to synthesize two-dimensional $CsPb_2Br_5$ nano-/micro-sheets for high-performance solution-processed photodetectors. Journal of Alloys and Compounds, 2020, 824: 153970
159. Passarelli J V, Fairfield D J, Sather N A, Hendricks M P, Sai H, Stern C L, Stupp S I. Enhanced out-of-plane conductivity and photovoltaic performance in $n = 1$ layered perovskites through organic cation design. Journal of the American Chemical Society, 2018, 140(23): 7313–7323
160. Van Gompel W T M, Herckens R, Van Hecke K, Ruttens B, D'Haen J, Lutsen L, Vanderzande D. Towards 2D layered hybrid perovskites with enhanced functionality: introducing charge-transfer complexes via self-assembly. Chemical Communications (Cambridge), 2019, 55(17): 2481–2484
161. Gélvez-Rueda M C, Fridriksson M B, Dubey R K, Jager W F, van der Stam W, Grozema F C. Overcoming the exciton binding energy in two-dimensional perovskite nanoplatelets by attachment of conjugated organic chromophores. Nature Communications,

2020, 11(1): 1901

162. Yuan Y, Chae J, Shao Y, Wang Q, Xiao Z, Centrone A, Huang J. Photovoltaic switching mechanism in lateral structure hybrid perovskite solar cells. Advanced Energy Materials, 2015, 5(15): 1500615
163. Xiao Z, Yuan Y, Shao Y, Wang Q, Dong Q, Bi C, Sharma P, Gruverman A, Huang J. Giant switchable photovoltaic effect in organometal trihalide perovskite devices. Nature Materials, 2015, 14(2): 193–198
164. Juarez-Perez E J, Sanchez R S, Badia L, Garcia-Belmonte G, Kang Y S, Mora-Sero I, Bisquert J. Photoinduced giant dielectric constant in lead halide perovskite solar cells. Journal of Physical Chemistry Letters, 2014, 5(13): 2390–2394
165. Deng Y, Xiao Z, Huang J. Light-induced self-poling effect on organometal trihalide perovskite solar cells for increased device efficiency and stability. Advanced Energy Materials, 2015, 5(20): 1500721
166. Zhao Y, Wei J, Li H, Yan Y, Zhou W, Yu D, Zhao Q. A polymer scaffold for self-healing perovskite solar cells. Nature Communications, 2016, 7(1): 10228
167. Nie W, Blancon J C, Neukirch A J, Appavoo K, Tsai H, Chhowalla M, Alam M A, Sfeir M Y, Katan C, Even J, Tretiak S, Crochet J J, Gupta G, Mohite A D. Light-activated photocurrent degradation and self-healing in perovskite solar cells. Nature Communications, 2016, 7(1): 11574
168. Hoke E T, Slotcavage D J, Dohner E R, Bowring A R, Karunadasa H I, McGehee M D. Reversible photo-induced trap formation in mixed-halide hybrid perovskites for photovoltaics. Chemical Science (Cambridge), 2015, 6(1): 613–617
169. Lee J W, Kim S G, Yang J M, Yang Y, Park N G. Verification and mitigation of ion migration in perovskite solar cells. APL Materials, 2019, 7(4): 041111
170. Yang D, Li X, Zeng H. Surface chemistry of all inorganic halide perovskite nanocrystals: passivation mechanism and stability. Advanced Materials Interfaces, 2018, 5(8): 1701662
171. Li Z, Xiao C, Yang Y, Harvey S P, Kim D H, Christians J A, Yang M, Schulz P, Nanayakkara S U, Jiang C S, Luther J M, Berry J J, Beard M C, Al-Jassim M M, Zhu K. Extrinsic ion migration in perovskite solar cells. Energy & Environmental Science, 2017, 10(5): 1234–1242
172. Zhang H, Fu X, Tang Y, Wang H, Zhang C, Yu W W, Wang X, Zhang Y, Xiao M. Phase segregation due to ion migration in all-inorganic mixed-halide perovskite nanocrystals. Nature Communications, 2019, 10(1): 1088
173. Cho J, DuBose J T, Le A N T, Kamat P V. Suppressed halide ion migration in 2D lead halide perovskites. ACS Materials Letters, 2020, 2(6): 565–570
174. Zhao Y C, Zhou W K, Zhou X, Liu K H, Yu D P, Zhao Q. Quantification of light-enhanced ionic transport in lead iodide perovskite thin films and its solar cell applications. Light, Science & Applications, 2017, 6(5): e16243–e16248
175. Xing J, Wang Q, Dong Q, Yuan Y, Fang Y, Huang J. Ultrafast ion migration in hybrid perovskite polycrystalline thin films under light and suppression in single crystals. Physical Chemistry Chemical Physics, 2016, 18(44): 30484–30490
176. Lamberti F, Litti L, De Bastiani M, Sorrentino R, Gandini M, Meneghetti M, Petrozza A. High-quality, ligands-free, mixed-halide perovskite nanocrystals inks for optoelectronic applications. Advanced Energy Materials, 2017, 7(8): 1601703
177. Miao J, Zhang F. Recent progress on highly sensitive perovskite photodetectors. Journal of Materials Chemistry C, Materials for Optical and Electronic Devices, 2019, 7(7): 1741–1791
178. Yang Y, Dai H, Yang F, Zhang Y, Luo D, Zhang X, Wang K, Sun X W, Yao J. All-perovskite photodetector with fast response. Nanoscale Research Letters, 2019, 14(1): 291
179. Li C, Huang W, Gao L, Wang H, Hu L, Chen T, Zhang H. Recent advances in solution-processed photodetectors based on inorganic and hybrid photo-active materials. Nanoscale, 2020, 12(4): 2201–2227
180. Wang X, Li M, Zhang B, Wang H, Zhao Y, Wang B. Recent progress in organometal halide perovskite photodetectors. Organic Electronics, 2018, 52: 172–183
181. Saran R, Curry R J. Lead sulphide nanocrystal photodetector technologies. Nature Photonics, 2016, 10(2): 81–92
182. Fang Y, Dong Q, Shao Y, Yuan Y, Huang J. Highly narrowband perovskite single-crystal photodetectors enabled by surface-charge recombination. Nature Photonics, 2015, 9(10): 679–686
183. Gao L, Zeng K, Guo J, Ge C, Du J, Zhao Y, Chen C, Deng H, He Y, Song H, Niu G, Tang J. Passivated single-crystalline $CH_3NH_3PbI_3$ nanowire photodetector with high detectivity and polarization sensitivity. Nano Letters, 2016, 16(12): 7446–7454
184. Geng X, Wang F, Tian H, Feng Q, Zhang H, Liang R, Shen Y, Ju Z, Gou G Y, Deng N, Li Y T, Ren J, Xie D, Yang Y, Ren T L. Ultrafast photodetector by integrating perovskite directly on silicon wafer. ACS Nano, 2020, 14(3): 2860–2868
185. Fang Y, Huang J. Resolving weak light of sub-picowatt per square centimeter by hybrid perovskite photodetectors enabled by noise reduction. Advanced Materials, 2015, 27(17): 2804–2810
186. Dou L, Yang Y M, You J, Hong Z, Chang W H, Li G, Yang Y. Solution-processed hybrid perovskite photodetectors with high detectivity. Nature Communications, 2014, 5(1): 5404
187. Zeng J, Li X, Wu Y, Yang D, Sun Z, Song Z, Wang H, Zeng H. Space-confined growth of $CsPbBr_3$ film achieving photodetectors with high performance in all figures of merit. Advanced Functional Materials, 2018, 28(43): 1804394
188. Hu X, Zhang X, Liang L, Bao J, Li S, Yang W, Xie Y. High-performance flexible broadband photodetector based on organo-lead halide perovskite. Advanced Functional Materials, 2014, 24(46): 7373–7380
189. Baeg K J, Binda M, Natali D, Caironi M, Noh Y Y. Organic light detectors: photodiodes and phototransistors. Advanced Materials, 2013, 25(31): 4267–4295
190. Liu C, Wang K, Yi C, Shi X, Smith A W, Gong X, Heeger A J. Efficient perovskite hybrid photovoltaics via alcohol-vapor annealing treatment. Advanced Functional Materials, 2016, 26(1): 101–110
191. Hu W, Wu R, Yang S, Fan P, Yang J, Pan A. Solvent-induced crystallization for hybrid perovskite thin-film photodetector with high-performance and low working voltage. Journal of Physics. D, Applied Physics, 2017, 50(37): 375101
192. Cheng Z, Liu K, Yang J, Chen X, Xie X, Li B, Zhang Z, Liu L, Shan C, Shen D. High-performance planar-type ultraviolet

photodetector based on high-quality $CH_3NH_3PbCl_3$ perovskite single crystals. ACS Applied Materials & Interfaces, 2019, 11(37): 34144–34150

193. Wang F, Mei J, Wang Y, Zhang L, Zhao H, Zhao D. Fast photoconductive responses in organometal halide perovskite photodetectors. ACS Applied Materials & Interfaces, 2016, 8(4): 2840–2846
194. Shen Y, Yu D, Wang X, Huo C, Wu Y, Zhu Z, Zeng H. Two-dimensional $CsPbBr_3$/PCBM heterojunctions for sensitive, fast and flexible photodetectors boosted by charge transfer. Nanotechnology, 2018, 29(8): 085201
195. Li P, Shivananju B N, Zhang Y, Li S, Bao Q. High performance photodetector based on 2D $CH_3NH_3PbI_3$ perovskite nanosheets. Journal of Physics. D, Applied Physics, 2017, 50(9): 094002
196. Hu Q, Wu H, Sun J, Yan D, Gao Y, Yang J. Large-area perovskite nanowire arrays fabricated by large-scale roll-to-roll micro-gravure printing and doctor blading. Nanoscale, 2016, 8(9): 5350–5357
197. Liu J, Xue Y, Wang Z, Xu Z Q, Zheng C, Weber B, Song J, Wang Y, Lu Y, Zhang Y, Bao Q. Two-dimensional $CH_3NH_3PbI_3$ perovskite: synthesis and optoelectronic application. ACS Nano, 2016, 10(3): 3536–3542
198. Deng H, Dong D, Qiao K, Bu L, Li B, Yang D, Wang H E, Cheng Y, Zhao Z, Tang J, Song H. Growth, patterning and alignment of organolead iodide perovskite nanowires for optoelectronic devices. Nanoscale, 2015, 7(9): 4163–4170
199. Dong Y, Gu Y, Zou Y, Song J, Xu L, Li J, Xue J, Li X, Zeng H. Improving all-inorganic perovskite photodetectors by preferred orientation and plasmonic effect. Small, 2016, 12(40): 5622–5632
200. Li X, Yu D, Chen J, Wang Y, Cao F, Wei Y, Wu Y, Wang L, Zhu Y, Sun Z, Ji J, Shen Y, Sun H, Zeng H. Constructing fast carrier tracks into flexible perovskite photodetectors to greatly improve responsivity. ACS Nano, 2017, 11(2): 2015–2023
201. Ramasamy P, Lim D H, Kim B, Lee S H, Lee M S, Lee J S. All-inorganic cesium lead halide perovskite nanocrystals for photodetector applications. Chemical Communications, 2016, 52(10): 2067–2070
202. Li Y, Lv Y, Guo Z, Dong L, Zheng J, Chai C, Chen N, Lu Y, Chen C. One-step preparation of long-term stable and flexible CsPbBr3 perovskite quantum dots/ethylene vinyl acetate copolymer composite films for white light-emitting diodes. ACS Applied Materials & Interfaces, 2018, 10(18): 15888–15894
203. Jang D M, Kim D H, Park K, Park J, Lee J W, Song J K. Ultrasound synthesis of lead halide perovskite nanocrystals. Journal of Materials Chemistry C, Materials for Optical and Electronic Devices, 2016, 4(45): 10625–10629
204. Hamed M S, Mola G T. Mixed halide perovskite solar cells: progress and challenges. Critical Reviews in Solid State and Material Sciences, 2029, 45(2): 85–112
205. Ludwigs S, ed. P3HT Revisited-From Molecular Scale to Solar Cell Devices (Vol. 265). Berlin: Springer, 2014
206. Shockley W, Queisser H J. Detailed balance limit of efficiency of *p-n* junction solar cells. Journal of Applied Physics, 1961, 32(3): 510–519
207. Chen B, Yang M, Priya S, Zhu K. Origin of *J–V* hysteresis in perovskite solar cells. Journal of Physical Chemistry Letters, 2016, 7(5): 905–917
208. Li P, Zhang Y, Liang C, Xing G, Liu X, Li F, Liu X, Hu X, Shao G, Song Y. Phase pure 2D perovskite for high-performance 2D-3D heterostructured perovskite solar cells. Advanced Materials, 2018, 30(52): 1805323
209. Jena A K, Kulkarni A, Miyasaka T. Halide perovskite photovoltaics: background, status, and future prospects. Chemical Reviews, 2019, 119(5): 3036–3103
210. Yang W S, Park B W, Jung E H, Jeon N J, Kim Y C, Lee D U, Shin S S, Seo J, Kim E K, Noh J H, Seok S I. Iodide management in formamidinium-lead-halide-based perovskite layers for efficient solar cells. Science, 2017, 356(6345): 1376–1379
211. Snaith H. Perovskites: the emergence of a new era for low-cost, high-efficiency solar cells. Journal of Physical Chemistry Letters, 2013, 4(21): 3623–3630
212. Wurfel U, Cuevas A, Wurfel P. Charge carrier separation in solar cells. IEEE Journal of Photovoltaics, 2015, 5(1): 461–469
213. Zhou D, Zhou T, Tian Y, Zhu X, Tu Y. Perovskite-based solar cells: materials, methods, and future perspectives. Journal of Nanomaterials, 2018, 2018: 8148072
214. Calió L, Kazim S, Grätzel M, Ahmad S. Hole-transport materials for perovskite solar cells. Angewandte Chemie International Edition, 2016, 55(47): 14522–14545
215. Guo Z, Gao L, Zhang C, Xu Z, Ma T. Low-temperature processed non-TiO_2 electron selective layers for perovskite solar cells. Journal of Materials Chemistry A, Materials for Energy and Sustainability, 2018, 6(11): 4572–4589
216. Jeng J Y, Chiang Y F, Lee M H, Peng S R, Guo T F, Chen P, Wen T C. $CH_3NH_3PbI_3$ perovskite/fullerene planar-heterojunction hybrid solar cells. Advanced Materials, 2013, 25(27): 3727–3732
217. Yu J C, Hong J A, Jung E D, Kim D B, Baek S M, Lee S, Cho S, Park S S, Choi K J, Song M H. Highly efficient and stable inverted perovskite solar cell employing PEDOT:GO composite layer as a hole transport layer. Scientific Reports, 2018, 8(1): 1070
218. Fang Y, Bi C, Wang D, Huang J. The functions of fullerenes in hybrid perovskite solar cells. ACS Energy Letters, 2017, 2(4): 782–794
219. Bush K A, Palmstrom A F, Yu Z J, Boccard M, Cheacharoen R, Mailoa J P, McMeekin D P, Hoye R L Z, Bailie C D, Leijtens T, Peters I M, Minichetti M C, Rolston N, Prasanna R, Sofia S, Harwood D, Ma W, Moghadam F, Snaith H J, Buonassisi T, Holman Z C, Bent S F, McGehee M D. 23.6%-efficient monolithic perovskite/silicon tandem solar cells with improved stability. Nature Energy, 2017, 2(4): 17009
220. Swain B S, Lee J. Fabrication and optimization of nanocube mixed halide perovskite films for solar cell application. Solar Energy, 2020, 201: 209–218
221. Liu Q, Zhao Y, Ma Y, Sun X, Ge W, Fang Z, Bai H, Tian Q, Fan B, Zhang T. A mixed solvent for rapid fabrication of large-area methylammonium lead iodide layers by one-step coating at room temperature. Journal of Materials Chemistry A, Materials for Energy and Sustainability, 2019, 7(31): 18275–18284
222. Hou W, Xiao Y, Han G, Qin C, Xiao L, Chang Y, Li H. Dimethyl sulfoxide and bromide methylamine co-treatment inducing defect healing for effective and stable perovskite solar cells. Materials Research Bulletin, 2019, 112: 165–173

223. Lyu M, Chen J, Park N G. Improvement of efficiency and stability of CuSCN-based inverted perovskite solar cells by post-treatment with potassium thiocyanate. Journal of Solid State Chemistry, 2019, 269: 367–374
224. Wang X D, Li W G, Liao J F, Kuang D B. Recent advances in halide perovskite single-crystal thin films: fabrication methods and optoelectronic applications. Solar RRL, 2019, 3(4): 1800294
225. Zhang J, Zhai G, Gao W, Zhang C, Shao Z, Mei F, Zhang J, Yang Y, Liu X, Xu B. Accelerated formation and improved performance of $CH_3NH_3PbI_3$-based perovskite solar cells via solvent coordination and anti-solvent extraction. Journal of Materials Chemistry A, Materials for Energy and Sustainability, 2017, 5(8): 4190–4198
226. Xia Y, Ran C, Chen Y, Li Q, Jiang N, Li C, Pan Y, Li T, Wang J, Huang W. Management of perovskite intermediates for highly efficient inverted planar heterojunction perovskite solar cells. Journal of Materials Chemistry A, Materials for Energy and Sustainability, 2017, 5(7): 3193–3202
227. Zhou X, Zhang Y, Kong W, Hu M, Zhang L, Liu C, Li X, Pan C, Yu G, Cheng C, Xu B. Crystallization manipulation and morphology evolution for highly efficient perovskite solar cell fabrication *via* hydration water induced intermediate phase formation under heat assisted spin-coating. Journal of Materials Chemistry A, Materials for Energy and Sustainability, 2018, 6(7): 3012–3021
228. Ye F, Chen H, Xie F, Tang W, Yin M, He J, Bi E, Wang Y, Yang X, Han L. Soft-cover deposition of scaling-up uniform perovskite thin films for high cost-performance solar cells. Energy & Environmental Science, 2016, 9(7): 2295–2301
229. Hao F, Stoumpos C C, Guo P, Zhou N, Marks T J, Chang R P H, Kanatzidis M G. Solvent-mediated crystallization of $CH_3NH_3SnI_3$ films for heterojunction depleted perovskite solar cells. Journal of the American Chemical Society, 2015, 137(35): 11445–11452
230. Ma C, Shen D, Huang B, Li X, Chen W C, Lo M F, Wang P, Hon-Wah Lam M, Lu Y, Ma B, Lee C S. High performance low-dimensional perovskite solar cells based on a one dimensional lead iodide perovskite. Journal of Materials Chemistry A, Materials for Energy and Sustainability, 2019, 7(15): 8811–8817
231. You P, Tang G, Yan F. Two-dimensional materials in perovskite solar cells. Materials Today Energy, 2019, 11: 128–158
232. Wei Y, Chu H, Chen B, Tian Y, Yang X, Cai B, Zhang Y, Zhao J. Two-dimensional cyclohexane methylamine-based perovskites as stable light absorbers for solar cells. Solar Energy, 2020, 201: 13–20
233. Chang C Y, Tsai B C, Lin M Z, Huang Y C, Tsao C S. An integrated approach towards the fabrication of highly efficient and long-term stable perovskite nanowire solar cells. Journal of Materials Chemistry A, Materials for Energy and Sustainability, 2017, 5(43): 22824–22833
234. Wang S W, Yan S, Wang M A, Chang L, Wang J L, Wang Z. Construction of nanowire $CH_3NH_3PbI_3$-based solar cells with 17.62% efficiency by solvent etching technique. Solar Energy Materials and Solar Cells, 2017, 167: 173–177
235. Singh R, Suranagi S R, Yang S J, Cho K. Enhancing the power conversion efficiency of perovskite solar cells via the controlled growth of perovskite nanowires. Nano Energy, 2018, 51: 192–198
236. He J, Zhang F, Xiang Y, Lian J, Wang X, Zhang Y, Peng X, Zeng P, Qu J, Song J. Preparation of low dimensional antimonene oxides and their application in Cu:NiO_x based planar pin perovskite solar cells. Journal of Power Sources, 2019, 435: 226819
237. Sanehira E M, Marshall A R, Christians J A, Harvey S P, Ciesielski P N, Wheeler L M, Schulz P, Lin L Y, Beard M C, Luther J M. Enhanced mobility $CsPbI_3$ quantum dot arrays for record-efficiency, high-voltage photovoltaic cells. Science Advances, 2017, 3(10): eaao4204
238. Mao L, Wu Y, Stoumpos C C, Traore B, Katan C, Even J, Wasielewski M R, Kanatzidis M G. Tunable white-light emission in single-cation-templated three-layered 2D perovskites $(CH_3CH_2NH_3)_4Pb_3Br_{10-x}Cl_x$. Journal of the American Chemical Society, 2017, 139(34): 11956–11963
239. Lau C F J, Deng X, Zheng J, Kim J, Zhang Z, Zhang M, Bing J, Wilkinson B, Hu L, Patterson R, Huang S, Ho-Baillie A. Enhanced performance *via* partial lead replacement with calcium for a $CsPbI_3$ perovskite solar cell exceeding 13% power conversion efficiency. Journal of Materials Chemistry A, Materials for Energy and Sustainability, 2018, 6(14): 5580–5586
240. Li B, Zhang Y, Fu L, Yu T, Zhou S, Zhang L, Yin L. Surface passivation engineering strategy to fully-inorganic cubic $CsPbI_3$ perovskites for high-performance solar cells. Nature Communications, 2018, 9(1): 1076
241. Niezgoda J S, Foley B J, Chen A Z, Choi J J. Improved charge collection in highly efficient $CsPbBrI_2$ solar cells with light-induced dealloying. ACS Energy Letters, 2017, 2(5): 1043–1049
242. Mehdi H, Mhamdi A, Bouazizi A. Effect of perovskite precursor ratios and solvents volume on the efficiency of $MAPbI_{3-x}Cl_x$ mixed halide perovskite solar cells. Materials Science in Semiconductor Processing, 2020, 109: 104915
243. Guo N, Zhang T, Li G, Xu F, Qian X, Zhao Y. A simple fabrication of $CH_3NH_3PbI_3$ perovskite for solar cells using low-purity PbI_2. Journal of Semiconductors, 2017, 38(1): 014004
244. Yang F, Kamarudin M A, Zhang P, Kapil G, Ma T, Hayase S. Enhanced crystallization by methanol additive in antisolvent for achieving high-quality $MAPbI_3$ perovskite films in humid atmosphere. ChemSusChem, 2018, 11(14): 2348–2357
245. Aydin E, Troughton J, Bastiani M D, Ugur E, Sajjad M, Alzahrani A, Neophytou M, Schwingenschlögl U, Laquai F, Baran D, De Wolf S. Room-temperature-sputtered nanocrystalline nickel oxide as hole transport layer for p–i–n perovskite solar cells. ACS Applied Energy Materials, 2018, 1(11): 6227–6233
246. Guo Y, Yin X, Liu J, Chen W, Wen S, Que M, Xie H, Yang Y, Que W, Gao B. Vacuum thermal-evaporated SnO_2 as uniform electron transport layer and novel management of perovskite intermediates for efficient and stable planar perovskite solar cells. Organic Electronics, 2019, 65: 207–214
247. Park I J, Kang G, Park M A, Kim J S, Seo S W, Kim D H, Zhu K, Park T, Kim J Y. Highly efficient and uniform 1 cm^2 perovskite solar cells with an electrochemically deposited NiO_x hole-extraction layer. ChemSusChem, 2017, 10(12): 2660–2667
248. Yin G, Zhao H, Jiang H, Yuan S, Niu T, Zhao K, Liu Z, Liu S F. Precursor engineering for all-inorganic $CsPbI_2Br$ perovskite solar cells with 14.78% efficiency. Advanced Functional Materials, 2018, 28(39): 1803269

249. Jiang H, Feng J, Zhao H, Li G, Yin G, Han Y, Yan F, Liu Z, Liu S. Low temperature fabrication for high performance flexible $CsPbI_2Br$ perovskite solar cells. Advancement of Science, 2018, 5(11): 1801117
250. Mazzarella L, Lin Y H, Kirner S, Morales-Vilches A B, Korte L, Albrecht S, Crossland E, Stannowski B, Case C, Snaith H J, Schlatmann R. Infrared light management using a nanocrystalline silicon oxide interlayer in monolithic perovskite/silicon heterojunction tandem solar cells with efficiency above 25%. Advanced Energy Materials, 2019, 9(14): 1803241
251. Liu Z, Chang J, Lin Z, Zhou L, Yang Z, Chen D, Zhang C, Liu S, Hao Y. High-performance planar perovskite solar cells using low temperature, solution-combustion-based nickel oxide hole transporting layer with efficiency exceeding 20%. Advanced Energy Materials, 2018, 8(19): 1703432
252. Jo Y, Oh K S, Kim M, Kim K H, Lee H, Lee C W, Kim D S. High performance of planar perovskite solar cells produced from PbI_2 (DMSO) and PbI_2 (NMP) complexes by intramolecular exchange. Advanced Materials Interfaces, 2016, 3(10): 1500768
253. Gkini K E, Antoniadou M, Balis N, Kaltzoglou A, Kontos A G, Falaras P. Mixing cations and halide anions in perovskite solar cells. Materials Today: Proceedings, 2019, 19: 73–78
254. Jiang L L, Wang Z K, Li M, Zhang C C, Ye Q Q, Hu K H, Lu D Z, Fang P F, Liao L S. Passivated perovskite crystallization via g-C_3N_4 for high-performance solar cells. Advanced Functional Materials, 2018, 28(7): 1705875
255. Hadadian M, Correa-Baena J P, Goharshadi E K, Ummadisingu A, Seo J Y, Luo J, Gholipour S, Zakeeruddin S M, Saliba M, Abate A, Grätzel M, Hagfeldt A. Enhancing efficiency of perovskite solar cells via N-doped graphene: crystal modification and surface passivation. Advanced Materials, 2016, 28(39): 8681–8686
256. Swarnkar A, Marshall A R, Sanehira E M, Chernomordik B D, Moore D T, Christians J A, Chakrabarti T, Luther J M. Quantum dot-induced phase stabilization of α-$CsPbI_3$ perovskite for high-efficiency photovoltaics. Science, 2016, 354(6308): 92–95
257. Ahmad K, Kumar P, Mobin S M. A two-step modified sequential deposition method-based Pb-free $(CH_3NH_3)_3Sb_2I_9$ perovskite with improved open circuit voltage and performance. ChemElectroChem, 2020, 7(4): 946–950

Rashad Kahwagi received a M.Sc. degree in Chemical Engineering from the University of Balamand, Lebanon in 2018 and is currently pursuing a Ph.D. degree at Dalhousie University, Canada under the supervision of Prof. Ghada Koleilat. His research focus is mainly on the different treatment development for perovskite materials in solar cells, with a future concentration on various energy generator applications.

Sean Thornton received a B.Eng. degree in Environmental Engineering from Dalhousie University, Canada in 2019. He is currently a Ph.D. student in Chemical Engineering at Dalhousie University, Canada under the supervision of Prof. Ghada Koleilat. His research interest is low-dimensional organic-inorganic hybrid perovskite solar cells.

Ben Smith received a bachelor's degree in Materials Engineering from Dalhousie University, Canada and is currently pursuing a MASc in Chemical Engineering under the supervision of Prof. Ghada Koleilat. His current research interests focus on advanced materials in photovoltaic applications, including metal halide perovskites, and conductive polymer electrodes.

Prof. **Ghada Koleilat** received her BASc (2006) in Electrical Engineering from Concordia University, Canada, her MASc (2008) and her Ph.D. (2012) degrees in Electrical Engineering from the University of Toronto, Canada. During her graduate studies, she developed the world's first functional colloidal quantum dot tandem solar cell employing a single quantum tuned material. She also conceived a material processing that enabled prolonged stability and improved electrical properties in photovoltaic junctions based on colloidal quantum dots. Before joining Dalhousie University, Canada in August 2016, Koleilat did her postdoctoral training at Stanford University, USA where she investigated the properties of single walled carbon nanotubes and their potential in photovoltaics. She has received several prestigious highly competitive awards for her research work, most recently she was one of the first awardee of the New Frontiers in Research Fund (Exploration stream). Her group focuses on investigating the properties of advanced materials for use in energy conversion applications.